Validation of the DSS Kernel

Ji-Young Lim

Academic advisor:
Prof. Dr.-Ing. H. Siegfried Stiehl

Universität Hamburg
Fachbereich Informatik
Arbeitsbereich Kognitive Systeme

June, 2002

Abstract

In this work, first we consider the behavior of the derived DSS kernel w.r.t. smoothing and differentiation. We describe how to calculate the coefficients of the DSS kernel, and show that there exist two types of the DSS first-order differencing operator (i.e. the even- and odd-number-sized one). Then, in order to characterize the performance of the DSS kernel w.r.t. smoothing and differentiation, in comparison to the sampled Gaussian (SG) kernel, we carry out a validation study given three performance criteria, namely accuracy of approximation, fulfillment of the non-enhancement requirement, and accuracy of edge extraction. The result of our validation study shows that the DSS kernel does not only match the performance of the SG kernel but also clearly exhibits superior performance w.r.t. smoothing and differentiation.

Zusammenfassung

In dieser Arbeit untersuchen wir im Detail die Glättungs- und Differentiationseigenschaften des von uns entwickelten diskreten Skalenraumskerns (DSS-Kern). Wir beschreiben zunächst die Berechnung der Koeffizienten des DSS-Kerns und geben zwei Varianten für die Ableitungen erster Ordnung (gerader bzw. ungerader Kern) an. Wir vergleichen anschließend die Glättungs- und Differentiationseigenschaften des DSS-Kerns mit denen eines abgetasteten Gauß-Kerns (SG-Kern) anhand von drei verschiedenen Performanzkriterien: Approximationsgenauigkeit, Erfüllung der "non-enhancement"-Bedingung sowie Genauigkeit bei der Kantenextraktion. Unsere Untersuchung zeigt, dass der von uns entwickelte DSS-Kern dem SG-Kern bzgl. seiner Glättungs- und Differentiationseigenschaften überlegen ist.

Contents

1 Introduction

Supplementing the work by Lindeberg [13], we proposed an improved discrete scale-space formulation by way of a theoretically thorough derivation in [9] [11]. We call the derived discrete scale-space kernel "the DSS kernel".

In the first part of this report, we consider the behavior of the DSS kernel with respect to both smoothing and differentiation. The coefficients of the DSS kernel at a certain scale for smoothing are easily calculated using the z-transform. These are compared with those of the sampled Gaussian which we call "the SG kernel". Furthermore, in order to apply the DSS kernel to image structures for the purpose of feature extraction, it is necessary to derive the associated differencing operator. We show that there exist two types of the DSS first-order differencing operator, viz. the even- and odd-number-sized DSS first-order differencing kernels. We describe how to calculate their coefficients and investigate the related properties. The DSS first-order differencing kernels are then compared with the SG first-order differencing kernel.

As a next step, we propose a validation study of the DSS kernel in order to characterize its performance with respect to both smoothing and differentiation. Our validation study is based upon three performance criteria, namely accuracy of approximation, fulfillment of the non-enhancement requirement, and accuracy of edge extraction. The first two criteria are related to the performance of smoothing, while the last criterion is to the performance of differentiation. This (i.e. the criterion of accuracy of edge extraction) is divided into two subcriteria i.e. rotation invariance and steadiness from adjacency. The result of our validation study shows that the DSS kernel does not only match the performance of the SG kernel but also clearly exhibits superior performance with w.r.t. smoothing and differentiation.

This report is organized as follow: In Section 2, we describe the behavior of the DSS kernel with respect to smoothing as well as differentiation. In Section 3, we present the overview of our validation study and the experimental settings. Subsequently, we provide the results of the validation study, and assess them in Section 4. Finally, we give a conclusion in Section 5.

2 Behavior of the DSS Kernel

The DSS kernel is given by

$$T\left(x;\frac{k}{3}\right) = *^k \left(\frac{1}{6} \quad \frac{2}{3} \quad \frac{1}{6}\right), \tag{2.1}$$

where $*^k$ is denoted as k-times self-convolution and $\frac{k}{3}$ corresponds to the variance.

In the following sections, we describe how to calculate the coefficients of the DSS kernel for both smoothing and differentiation, and show the properties of the DSS kernel compared with the SG kernel.

2.1 Smoothing Kernel

2.1.1 In One Dimension

The coefficients of the DSS kernel generated by self-convolution given in Eq. 2.1 can be easily calculated using the z-transform of the given DSS kernel based on the property that convolution of sequences corresponds to multiplication of the z-transform (see for the detail e.g. [1], [5], [14], or [15]) such that

$$T\left(x;\frac{k}{3}\right) \circ\!\!-\!\!\bullet \left(\frac{1}{6}z^{-1} + \frac{2}{3} + \frac{1}{6}z\right)^k,$$

where k is the number of self-convolution.

The DSS kernels of increasing variance are given in Tab. 2.1, whereas the SG kernels (of equal variance and with the same number of coefficients) are given in Tab. 2.2, where the number of the coefficients equals $2k+1$. Through a comparison of the values in Tab. 2.1 with those in Tab. 2.2, one can see that the DSS kernels are normalized to one for any k, whereas the SG kernels are not normalized when the variance is small. Furthermore, the coefficients of the DSS kernel are getting similar to those of the SG kernel as the variance increases.

Tab. 2.3 gives a comparison between the DSS kernel and the SG kernel for smoothing.

k	$T\left(x;\frac{k}{3}\right) \circ\!\!-\!\!\bullet \left(\frac{1}{6}z^{-1}+\frac{2}{3}+\frac{1}{6}z\right)^k$	Sum of coef.
1	$\{\frac{1}{6} \quad \frac{2}{3} \quad \frac{1}{6}\}$	1
2	$\{\frac{1}{36} \quad \frac{2}{9} \quad \frac{1}{2} \quad \frac{2}{9} \quad \frac{1}{36}\}$	1
3	$\{\frac{1}{216} \quad \frac{1}{18} \quad \frac{17}{72} \quad \frac{11}{27} \quad \frac{17}{72} \quad \frac{1}{18} \quad \frac{1}{216}\}$	1
4	$\{\frac{1}{1296} \quad \frac{1}{81} \quad \frac{25}{324} \quad \frac{19}{81} \quad \frac{227}{648} \quad \frac{19}{81} \quad \frac{25}{324} \quad \frac{1}{81} \quad \frac{1}{1296}\}$	1
5	$\{\frac{1}{7776} \quad \frac{5}{1944} \quad \frac{55}{2592} \quad \frac{5}{54} \quad \frac{295}{1296} \quad \frac{101}{324} \quad \frac{295}{1296} \quad \frac{5}{54} \quad \frac{55}{2592} \quad \frac{5}{1944} \quad \frac{1}{7776}\}$	1
6	$\{\frac{1}{46656} \quad \frac{1}{1944} \quad \frac{41}{7776} \quad \frac{175}{5832} \quad \frac{535}{5184} \quad \frac{71}{324} \quad \frac{1103}{3888} \quad \frac{71}{324} \quad \frac{535}{5184} \quad \frac{175}{5832} \quad \frac{41}{7776} \quad \frac{1}{1944} \quad \frac{1}{46656}\}$	1

Table 2.1: Coefficients of the 1-D DSS kernel.

k	$SG\left(x;\frac{k}{3}\right) = \{G(x;t) = \frac{1}{\sqrt{2\pi t}}e^{-\frac{x^2}{2t}}\} \quad \left(t=\frac{k}{3}\right)$	Sum of coef.
1	{0.15418 0.69099 0.15418}	0.99935
2	{0.02433 0.23080 0.48860 0.23080 0.02433}	0.99885
3	{0.00443 0.05399 0.24197 0.39894 0.24197 0.05399 0.00443}	0.99973
4	{0.00086 0.01182 0.07709 0.23745 0.34549 0.23745 0.07709 0.01182 0.00086}	0.99994
5	{0.00017 0.00254 0.02077 0.09307 0.22893 0.30902 0.22893 0.09307 0.02077 0.00254 0.00017}	0.99999
6	{0.00003 0.00054 0.00517 0.02973 0.10378 0.21970 0.28209 0.21970 0.10378 0.02973 0.00517 0.00054 0.00003}	1.0

Table 2.2: Coefficients of the 1-D SG kernel.

	The DSS kernel	The SG kernel
Getting coefficients	Through a self-convolution	Sampling the Gaussian
Number of coefficients	$2k+1$ ($k \in \mathbb{Z}_+$: the number of self-convolution)	
Variance	$\frac{k}{3}$	
Semi-group property	Satisfied	
Symmetry	Yes	
Normalization	Always for any k	Not always

(a) Properties

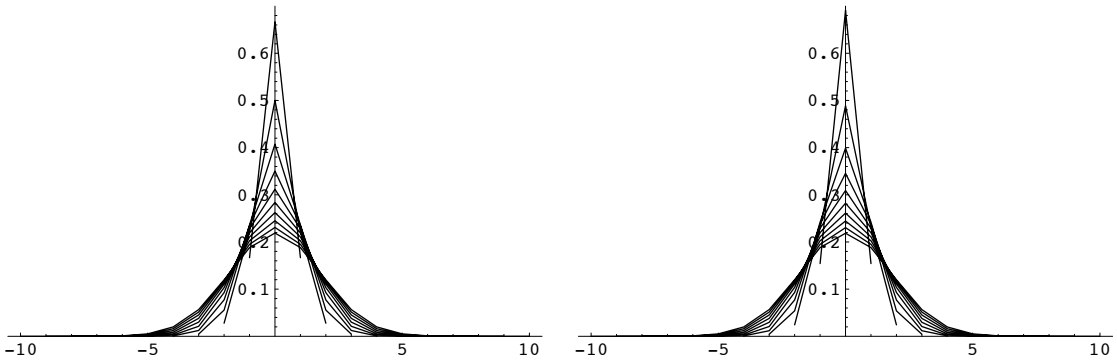

$T\left(x;\frac{k}{3}\right)$ $SG\left(x;\frac{k}{3}\right)$

(b) Graphical illustration ($k = 1, 2, \cdots, 10$)

Table 2.3: Comparison of the DSS kernel with the SG kernel for smoothing.

2.1.2 In Higher Dimensions

Based on the separability of the higher dimensional DSS kernel, for $\vec{x} = \{x_1, x_2, \cdots, x_N\}$

$$T(\vec{x};\cdot) = T(x_1;\cdot) * T(x_2;\cdot) * \cdots * T(x_N;\cdot) \tag{2.2}$$

holds, where '*' denotes convolution. For example, the smallest 2-D DSS kernel is given by

$$\begin{aligned} T\left(x, y; \frac{1}{3}\right) &= T\left(x; \frac{1}{3}\right) * T\left(y; \frac{1}{3}\right) \\ &= \begin{pmatrix} \frac{1}{6} & \frac{2}{3} & \frac{1}{6} \end{pmatrix}_x * \begin{pmatrix} \frac{1}{6} & \frac{2}{3} & \frac{1}{6} \end{pmatrix}_y, \end{aligned}$$

the coefficients of which can be easily calculated using its z-transform

$$T\left(x; \frac{1}{3}\right) * T\left(y; \frac{1}{3}\right) \circ\!\!-\!\!\bullet \left(\frac{1}{6}z^{-1} + \frac{2}{3} + \frac{1}{6}z\right) \cdot \left(\frac{1}{6}\omega^{-1} + \frac{2}{3} + \frac{1}{6}\omega\right) \bullet\!\!-\!\!\circ \begin{pmatrix} \frac{1}{36} & \frac{1}{9} & \frac{1}{36} \\ \frac{1}{9} & \frac{4}{9} & \frac{1}{9} \\ \frac{1}{36} & \frac{1}{9} & \frac{1}{36} \end{pmatrix}.$$

The higher dimensional DSS kernel with larger variance, analogously to 1-D, can be derived through self-convolution which corresponds to multiplication in the z-transform such that

$$T\left(x, y; \frac{k}{3}\right) = *^k T\left(x, y; \frac{1}{3}\right) \circ\!\!-\!\!\bullet \left(\frac{1}{6}z^{-1} + \frac{2}{3} + \frac{1}{6}z\right)^k \cdot \left(\frac{1}{6}\omega^{-1} + \frac{2}{3} + \frac{1}{6}\omega\right)^k,$$

where k denotes the number of self-convolution. Tab. 2.4 gives a graphical illustration of the 2-D DSS kernels of increasing variance ($k = 1, 2, \cdots, 10$) that can be compared with the 2-D SG kernels given by Tab. 2.5.

2.2 Differencing Kernel

In order to apply the DSS kernel to image structures for the purpose of feature extraction, it is necessary to derive its derivative operator. Differently from the continuous case in which any nth-order derivatives of the Gaussian can be defined at any scale, it is not as simple to define the derivative operator in the discrete case. By introducing the terminology "differencing operator" denoted as $\triangle$, we here discriminate the discrete derivative from the continuous derivative.

$T\left(x, y; \frac{k}{3}\right) \quad (k = 1, 2, \cdots, 10)$
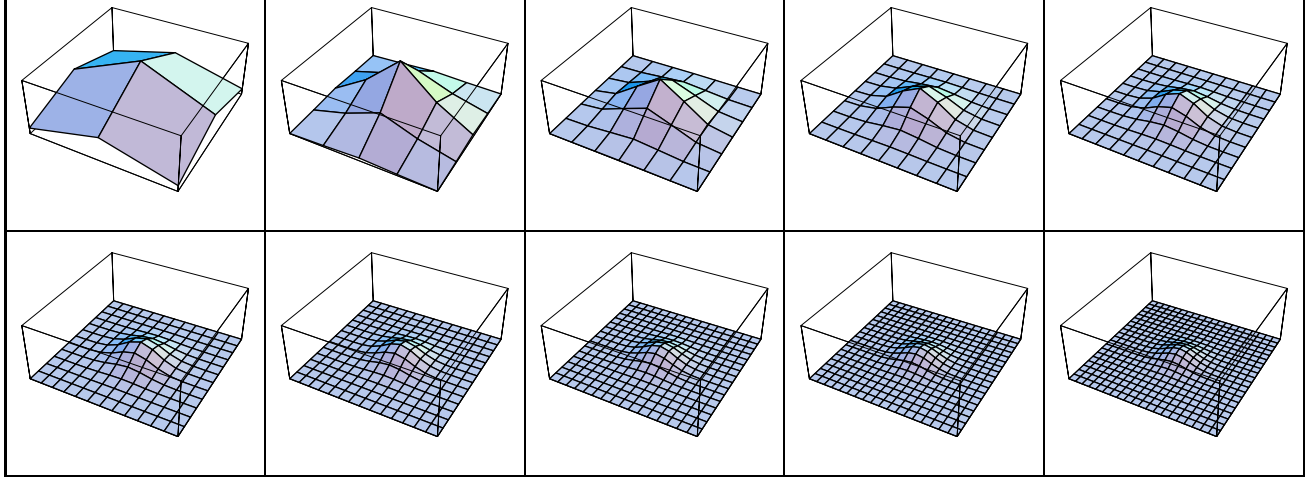

Table 2.4: Graphical illustration of the 2-D DSS kernel.

$SG\left(x, y; \frac{k}{3}\right) \quad (k = 1, 2, \cdots, 10)$
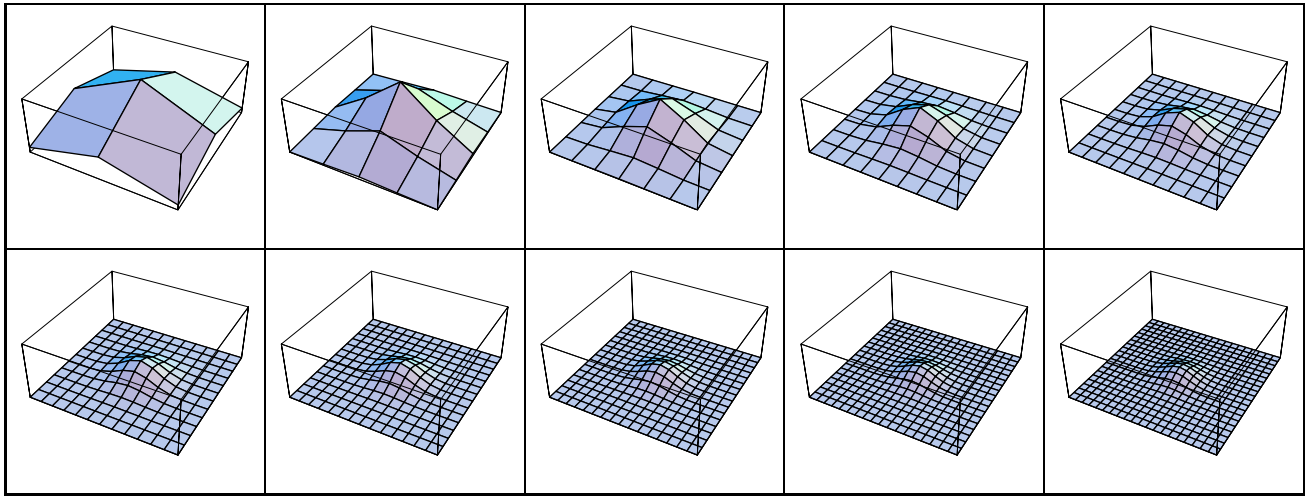

Table 2.5: Graphical illustration of the 2-D SG kernel.

In the following subsections, we describe how to derive the DSS first-order differencing operator (note that we consider the first-order differencing operator only), and look into its properties.

2.2.1 Calculation of the DSS Differencing Kernel

A function has to be differentiated numerically when the analytical solution cannot be determined at all ([2], [7]). Based on the principles of numerical differentiation, one can approximate the derivatives by the difference quotient, for which there exist two formulae according to the number of points involved in the differencing:

1. Two-point difference formula denoted as $\triangle_{even}$

$$\begin{aligned} f_{\triangle_{even}}(x) &= \frac{f(x) - f(x-h)}{h} \\ &= f(x) - f(x-1) \quad (h = 1). \end{aligned}$$

2. Three-point difference formula denoted as $\triangle_{odd}$

$$\begin{aligned} f_{\triangle_{odd}}(x) &= \frac{f(x+h) - f(x-h)}{2h} \\ &= \frac{f(x+1) - f(x-1)}{2} \quad (h = 1). \end{aligned}$$

Based on these two formulae, we derive two types of the DSS first-order differencing operator using the z-transform:

1. The z-transform of $\triangle_{even}$ is given by

$$f_{\triangle_{even}}(x) = f(x) - f(x-1) \circ\!\!-\!\!\bullet\, F(z) \cdot (1 - z),$$

where $F(z)$ corresponds to the z-transform of $f(x)$. The DSS first-order differencing kernel through application of $\triangle_{even}$ is given by

$$T_{\triangle_{even}}\left(x; \frac{k}{3}\right) \circ\!\!-\!\!\bullet \left(\frac{1}{6}z^{-1} + \frac{2}{3} + \frac{1}{6}z\right)^k (1 - z) \bullet\!\!-\!\!\circ\, *^k \left\{\frac{1}{6}\ \frac{2}{3}\ \frac{1}{6}\right\} * \{1\ -1\}$$

from which, for example, the smallest DSS first-order even-number-sized differencing kernel (i.e. $k = 1$) is derived as follows

$$T_{\triangle_{even}}\left(x; \frac{1}{3}\right) \circ\!\!-\!\!\bullet \left(\frac{1}{6}z^{-1} + \frac{1}{2} - \frac{1}{2}z - \frac{1}{6}z^{2}\right) \bullet\!\!-\!\!\circ \left\{\frac{1}{6}\ \frac{1}{2}\ \frac{-1}{2}\ \frac{-1}{6}\right\}.$$

2. Analogously to $\triangle_{even}$, the z-transform of $\triangle_{odd}$ is given by

$$f_{\triangle_{odd}}(x) = \frac{f(x+1) - f(x-1)}{2} \circ\!\!-\!\!\bullet F(z) \cdot \left(\frac{1}{2}z^{-1} - \frac{1}{2}z\right),$$

and the DSS first-order differencing kernel through application of $\triangle_{odd}$ is given by

$$T_{\triangle_{odd}}\left(x; \frac{k}{3}\right) \circ\!\!-\!\!\bullet \left(\frac{1}{6}z^{-1} + \frac{2}{3} + \frac{1}{6}z\right)^{k} \left(\frac{1}{2}z^{-1} - \frac{1}{2}z\right) \bullet\!\!-\!\!\circ *^{k} \left\{\frac{1}{6}\ \frac{2}{3}\ \frac{1}{6}\right\} * \left\{\frac{1}{2}\ 0\ \frac{-1}{2}\right\}$$

from which, for example, the smallest DSS first-order odd-number-sized differencing kernel (i.e. $k = 1$) is derived as follows

$$T_{\triangle_{odd}}\left(x; \frac{1}{3}\right) \circ\!\!-\!\!\bullet \left(\frac{1}{12}z^{-2} + \frac{1}{3}z^{-1} - \frac{1}{3}z - \frac{1}{12}z^{2}\right) \bullet\!\!-\!\!\circ \left\{\frac{1}{12}\ \frac{1}{3}\ 0\ \frac{-1}{3}\ \frac{-1}{12}\right\}.$$

Since the DSS kernel is odd-number-sized (i.e. $2k + 1$ coefficients), the DSS first-order differencing kernel through application of $\triangle_{even}$ is even-number-sized, whereas that through application of $\triangle_{odd}$ is odd-number-sized. In Tab. 2.6, the coefficients of the DSS first-order even- and odd-number-sized differencing kernels compared with those of the SG first-order differencing kernel with increasing variance are given. Also, they are graphically illustrated as k increases in Fig. 2.1.

2.2.2 Properties of the DSS Differencing Kernel

Normalization

Let us assume that i) $f(x)$ is a scale-space kernel, ii) $f(x)$ should be sufficiently smooth so that n-th order derivatives can be taken, and iii) $f(x)$ is normalized such that $\int_x f(x)\, dx = 1$. Additionally, $f(x)$ is assumed to be essentially compact, meaning that it and all of its derivatives vanish sufficiently fast when $|x|$ goes to infinity, where "sufficiently fast"

k	$T_{\triangle_{even}}\left(x;\frac{k}{3}\right) \circ\!\!-\!\!\bullet \left(\frac{1}{6}z^{-1}+\frac{2}{3}+\frac{1}{6}z\right)^k\cdot(1-z)$	$T_{\triangle_{odd}}\left(x;\frac{k}{3}\right) \circ\!\!-\!\!\bullet \left(\frac{1}{6}z^{-1}+\frac{2}{3}+\frac{1}{6}z\right)^k\cdot(\frac{1}{2}z^{-1}-\frac{1}{2}z)$
1	$\{\frac{1}{6}\ \frac{1}{2}\ \frac{-1}{2}\ \frac{-1}{6}\}$	$\{\frac{1}{12}\ \frac{1}{3}\ 0\ \frac{-1}{3}\ \frac{-1}{12}\}$
2	$\{\frac{1}{36}\ \frac{7}{36}\ \frac{5}{18}\ \frac{-5}{18}\ \frac{-7}{36}\ \frac{-1}{36}\}$	$\{\frac{1}{72}\ \frac{1}{9}\ \frac{17}{72}\ 0\ \frac{-17}{72}\ \frac{-1}{9}\ \frac{-1}{72}\}$
3	$\{\frac{1}{216}\ \frac{11}{216}\ \frac{13}{72}\ \frac{37}{216}\ \frac{-37}{216}\ \frac{-13}{72}\ \frac{-11}{216}\ \frac{-1}{216}\}$	$\{\frac{1}{432}\ \frac{1}{36}\ \frac{25}{216}\ \frac{19}{108}\ 0\ \frac{-19}{108}\ \frac{-25}{216}\ \frac{-1}{36}\ \frac{-1}{432}\}$
4	$\{\frac{1}{1296}\ \frac{5}{432}\ \frac{7}{108}\ \frac{17}{108}\ \frac{25}{216}\ \frac{-25}{216}\ \frac{-17}{108}\ \frac{-7}{108}\ \frac{-5}{432}\ \frac{-1}{1296}\}$	$\{\frac{1}{2592}\ \frac{1}{162}\ \frac{11}{288}\ \frac{1}{9}\ \frac{59}{432}\ 0\ \frac{-59}{432}\ \frac{-1}{9}\ \frac{-11}{288}\ \frac{-1}{162}\ \frac{-1}{2592}\}$
5	$\{\frac{1}{7776}\ \frac{19}{7776}\ \frac{145}{7776}\ \frac{185}{2592}\ \frac{175}{1296}\ \frac{109}{1296}\ \frac{-109}{1296}\ \frac{-175}{1296}\ \frac{-185}{2592}\ \frac{-145}{7776}\ \frac{-19}{7776}\ \frac{-1}{7776}\}$	$\{\frac{1}{15552}\ \frac{5}{3888}\ \frac{41}{3888}\ \frac{175}{3888}\ \frac{535}{5184}\ \frac{71}{648}\ 0\ \frac{-71}{648}\ \frac{-535}{5184}\ \frac{-175}{3888}\ \frac{-41}{3888}\ \frac{-5}{3888}\ \frac{-1}{15552}\}$
6	$\{\frac{1}{46656}\ \frac{23}{46656}\ \frac{37}{7776}\ \frac{577}{23328}\ \frac{3415}{46656}\ \frac{601}{5184}\ \frac{251}{3888}\ \frac{-251}{3888}\ \frac{-601}{5184}\ \frac{-3415}{46656}\ \frac{-577}{23328}\ \frac{-37}{7776}\ \frac{-23}{46656}\ \frac{-1}{46656}\}$	$\{\frac{1}{93312}\ \frac{1}{3888}\ \frac{245}{93312}\ \frac{43}{2916}\ \frac{1523}{31104}\ \frac{1103}{11664}\ \frac{2807}{31104}\ 0\ \frac{-2807}{31104}\ \frac{-1103}{11664}\ \frac{-1523}{31104}\ \frac{-43}{2916}\ \frac{-245}{93312}\ \frac{-1}{3888}\ \frac{-1}{93312}\}$

(a) The DSS first-order even-number-sized (left) and odd-number-sized (right) differencing kernels

k	$SG_{\triangle}\left(x;\frac{k}{3}\right)=\{\frac{dG(x;t)}{dx}=\frac{-x}{t\sqrt{2\pi t}}e^{-\frac{x^2}{2t}}\}\quad(t=\frac{k}{3})$
1	{0.010277 0.462541 0 −0.462541 −0.010277}
2	{0.002574 0.072978 0.346199 0 −0.346199 −0.072978 −0.002574}
3	{0.000535 0.013296 0.107982 0.241971 0 −0.241971 −0.107982 −0.013296 −0.000535}
4	{0.000110 0.002569 0.026600 0.115635 0.178091 0 −0.178091 −0.115635 −0.026600 −0.002569 −0.000110}
5	{0.000023 0.000513 0.006104 0.037382 0.111690 0.137356 0 −0.137356 −0.111690 −0.037382 −0.006104 −0.000513 −0.000023}
6	{0.000005 0.000104 0.001361 0.010333 0.044599 0.103777 0.109848 0 −0.109848 −0.103777 −0.044599 −0.010333 −0.001361 −0.000104 −0.000005}

(b) The SG first-order differencing kernels

Table 2.6: Coefficients of the discrete first-order differencing kernels.

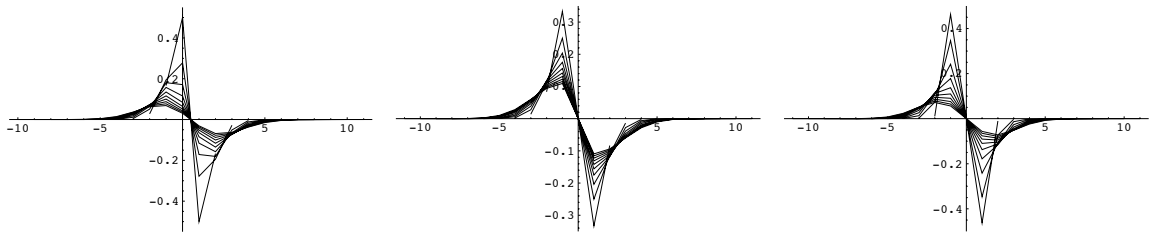

(a) $T_{\triangle_{even}}\left(x;\frac{k}{3}\right)$ (b) $T_{\triangle_{odd}}\left(x;\frac{k}{3}\right)$ (c) $SG_{\triangle}\left(x;\frac{k}{3}\right)$

Figure 2.1: Graphical illustration of the discrete first-order differencing kernels in 1-D ($k = 1, 2, \cdots 10$).

implies that faster than any polynomial factor could counteract (see for details [6]). Based on these assumptions, then, $f(x)$ simply follows by partial integration[1]:

$$
\begin{aligned}
1 &= \int_x f(x)\,dx = xf(x) - \int_x xf'(x)\,dx \\
&= xf(x) - \frac{1}{2}x^2 f'(x) + \frac{1}{2}\int_x x^2 f''(x)\,dx \\
&= xf(x) - \frac{1}{2}x^2 f'(x) + \frac{1}{2}\cdot\frac{1}{3}x^3 f''(x) - \frac{1}{2}\cdot\frac{1}{3}\int_x x^3 f^{(3)}(x)\,dx \\
&= xf(x) - \frac{1}{2}x^2 f'(x) + \frac{1}{2}\cdot\frac{1}{3}x^3 f''(x) - \frac{1}{2}\cdot\frac{1}{3}\left(\frac{1}{4}x^4 f^{(3)}(x) - \int_x \frac{1}{4}x^4 f^{(4)}(x)\,dx\right) \\
&\;\;\vdots \\
&= \int_x \frac{(-1)^n}{n!}x^n f^{(n)}(x)\,dx,
\end{aligned}
$$

[1]The partial integral rule reads [2])

$$\int uv'\,dx = uv - \int u'v\,dx.$$

where n is the order of the derivative. According to this rule, in the case of the first-order derivative (i.e. $n = 1$),

$$\int_x -xf'(x)\,dx = 1 \tag{2.3}$$

must hold.

Now let us examine whether the DSS first-order even- and odd-number-sized differencing kernels as well as the SG first-order differencing kernel satisfy the normalization requirement for the first-order derivative given by Eq. 2.3. In case of $T_{\triangle_{even}}(x; \frac{k}{3})$,

$$\begin{aligned}
\sum_x -x \cdot T_{\triangle_{even}}\left(x; \frac{1}{3}\right) &= -(-1)\cdot\frac{1}{6} + 0\cdot\frac{1}{2} - 1\cdot\frac{-1}{2} - 2\cdot\frac{-1}{6} = 1 \\
\sum_x -x \cdot T_{\triangle_{even}}\left(x; \frac{2}{3}\right) &= -(-2)\cdot\frac{1}{36} - (-1)\cdot\frac{7}{36} + 0\cdot\frac{5}{18} - 1\cdot\frac{-5}{18} - 2\cdot\frac{-7}{36} + 3\cdot\frac{-1}{36} = 1 \\
&\vdots \\
\sum_x -x \cdot T_{\triangle_{even}}\left(x; \frac{k}{3}\right) &= 1,
\end{aligned}$$

from which it is clear that normalization requirement is always fulfilled for any k. In case of $T_{\triangle_{odd}}(x; \frac{k}{3})$,

$$\begin{aligned}
\sum_x -x \cdot T_{\triangle_{odd}}\left(x; \frac{1}{3}\right) &= -(-2)\cdot\frac{1}{12} - (-1)\cdot\frac{1}{3} - 1\cdot\frac{-1}{3} - 2\cdot\frac{-1}{12} = 1 \\
\sum_x -x \cdot T_{\triangle_{odd}}\left(x; \frac{2}{3}\right) &= -(-3)\cdot\frac{1}{72} - (-2)\cdot\frac{1}{9} - (-1)\cdot\frac{17}{72} - 1\cdot\frac{-17}{72} - 2\cdot\frac{-1}{9} + 3\cdot\frac{-1}{72} = 1 \\
&\vdots \\
\sum_x -x \cdot T_{\triangle_{odd}}\left(x; \frac{k}{3}\right) &= 1,
\end{aligned}$$

which shows normalization requirement is also satisfied for any k. In the same way, we

examine the normalization of the SG first-order differencing kernel such that

$$\begin{aligned}
\sum_x -x \cdot SG_{\triangle}\left(x; \frac{1}{3}\right) &= 2\left(2 \cdot 0.010277 + 1 \cdot 0.462541\right) = 0.96619 \\
\sum_x -x \cdot SG_{\triangle}\left(x; \frac{2}{3}\right) &= 2\left(3 \cdot 0.002574 + 2 \cdot 0.072978 + 0.346199\right) = 0.999754 \\
&\vdots \\
\sum_x -x \cdot T_{\triangle_{odd}}\left(x; \frac{k}{3}\right) &\approxeq 1,
\end{aligned}$$

where one can see that $SG_{\triangle}(x; \frac{k}{3})$ is not perfectly normalized to one when the variance is small, although it converges to one as the variance increases.

Variance

The variance of $f(x)$ given by the second central moment (assuming it exists) can be written as the integral ([4])

$$\mathrm{Var}(f(x)) = \int_{-\infty}^{\infty} x^2 f(x)\, dx,$$

if the mean of $f(x)$ is zero. However, in case that $f(x)$ is asymmetric, i.e,

$$\begin{aligned}
&\int_{-\infty}^{\infty} f(x)\, dx = 0, \\
&\int_{-\infty}^{\infty} |f(x)|\, dx = 2\int_{-\infty}^{0} |f(x)|\, dx = 2\int_{0}^{\infty} |f(x)|\, dx,
\end{aligned}$$

the variance should be defined as

$$\mathrm{Var}(f(x)) = \int_{\infty}^{\infty} x^2 |f(x)|\, dx \tag{2.4}$$

in order to measure a dispersion of $f(x)$ (otherwise, it always corresponds to zero). Eq. 2.4 is a more generalized definition of variance.

For the case of the (continuous) Gaussian, according to the definition of Eq. 2.4, the variance of the Gaussian and that of the first-order derivative of the Gaussian are calculated

as

$$\mathrm{Var}(G(x;t)) = \int_{\infty}^{\infty} x^2 |G(x;t)|\, dx = \frac{x^2}{\sqrt{2\pi t}} e^{-\frac{x^2}{2t}}\, dx = t,$$
$$\mathrm{Var}\left(\frac{dG(x;t)}{dx}\right) = \int_{\infty}^{\infty} x^2 |G_x(x;t)|\, dx = 2\int_{0}^{\infty} \frac{x^3}{t\sqrt{2\pi t}} e^{-\frac{x^2}{2t}}\, dx = \frac{4}{2\pi}\sqrt{t}.$$

The variance of (of even- and odd-number-sized) $T_{\triangle}(x;t)$ can be calculated based on the definition of Eq. 2.4 as

$$\mathrm{Var}\left(T_{\triangle}(x;t)\right) = \sum_{x} x^2 \left|T_{\triangle}(x;t)\right|,$$

where t corresponds to the variance of $T(x;t)$ (see for the detail of calculating the variance of the DSS kernel [11, Sec. 2]) and t equals $\frac{k}{3}$ (k is the number of self-convolution). The variance of the $SG_{\triangle}(x;t)$ is derived in the same way.

Tab. 2.7(a) gives the variance of $G_x(x;t)$ (in the left column), of $SG_{\triangle}(x;t)$ (in the middle column), and of $T_{\triangle}(x;t)$ (in the right column), as t increases. Tab. 2.7(b) illustrates $\mathrm{Var}(G(x;t))$ versus $\mathrm{Var}(G_x(x;t))$ (in the left) and $\mathrm{Var}(T(x;t))$ versus $\mathrm{Var}(T_{\triangle}(x;t))$ (in the right). From Tab. 2.7, one can conclude several interesting points: (i) the variance of the Gaussian is not equivalent to that of its first-order derivative, (ii) $\mathrm{Var}(T_{\triangle_{even}}(x;t))$ equals $\mathrm{Var}(T_{\triangle_{odd}}(x;t))$ for any t, (iii) the variance of $SG_{\triangle}(x;t)$ is not identical with that of $G_x(x;t)$, though the former converges to the latter as t increases, and (iv) the graphical illustration of $\mathrm{Var}(T(x;t))$ versus $\mathrm{Var}(T_{\triangle}(x;t))$ looks quite similar to that of $\mathrm{Var}(G(x;t))$ versus $\mathrm{Var}(G_x(x;t))$.

Integration

Now, we are to consider the "integration kernel" corresponding to the DSS first-order differencing kernels (i.e. $T_{\triangle_{even}}$ and $T_{\triangle_{odd}}$) derived in Section 2.2.1.

For a given z-transformed DSS kernel $T(z)$ (i.e. $T(z) \bullet\!\!-\!\!\circ\, T(x)$), $T_{\triangle}(z)$ is derived from multiplying $T(z)$ with $\triangle_z$, which means that $T(z)$ is obtained by multiplying $T_{\triangle}(z)$ with $\triangle_z^{-1}$ such that

$$T_{\triangle}(z) \cdot \triangle_z^{-1} = T(z) \cdot \triangle_z \cdot \triangle_z^{-1} = T(z).$$

$t = \frac{k}{3}$	$\mathrm{Var}(G_x(x;t))$	$\mathrm{Var}(SG_{\triangle}(x;t))$	$\mathrm{Var}(T_{\triangle_{even}}(x;t))$	$\mathrm{Var}(T_{\triangle_{odd}}(x;t))$
$\frac{1}{3}$	0.92132	1.007296	1.333333	
$\frac{2}{3}$	1.30294	1.322564	1.611111	
1	1.59577	1.604247	1.851852	
$\frac{4}{3}$	1.84264	1.847769	2.066358	
$\frac{5}{3}$	2.06013	2.063693	2.261317	
2	2.25676	2.259416	2.441101	
$\frac{7}{3}$	2.43758	2.439653	2.608711	
$\frac{8}{3}$	2.60588	2.607557	2.766293	
3	2.76395	2.765244	2.915439	
$\frac{10}{3}$	2.91346	2.914640	3.057364	
$\frac{11}{3}$	3.05567	3.056679	3.193020	
4	3.19154	3.192422	3.323165	

(a) Variance values

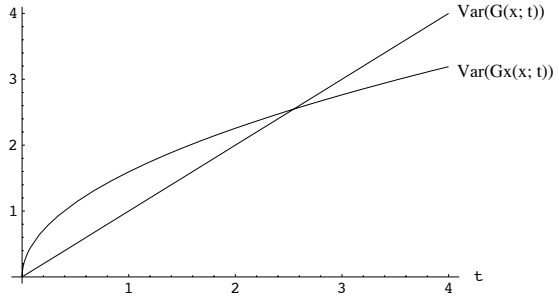

$\mathrm{Var}(G(x;t))$ vs. $\mathrm{Var}(G_x(x;t))$

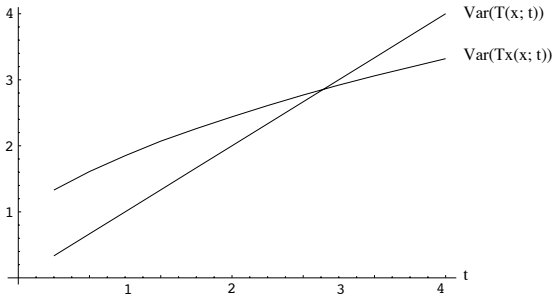

$\mathrm{Var}(T(x;t))$ vs. $\mathrm{Var}(T_{\triangle}(x;t))$

(b) Graphical illustration

Table 2.7: Variance of the first-order differencing kernels

Introducing a symbol ▲ that stands for $\triangle^{-1}$, we denote ▲ as the "discrete integration operator". Multiplication of $\blacktriangle_z$ corresponds to convolution of ▲ in the spatial domain. Since there exist two types of $\triangle_z$ (i.e. $\triangle_{even,z}$ and $\triangle_{odd,z}$), there are correspondingly two types of $\blacktriangle_z$ (i.e. $\blacktriangle_{even,z}$ and $\blacktriangle_{odd,z}$).

$\blacktriangle_{even,z}$ is given by

$$\blacktriangle_{even,z} = (\triangle_{even,z})^{-1} = (1-z)^{-1},$$

and the inverse transform[2] of $\blacktriangle_{even,z}$ is

$$\blacktriangle_{even,z} = \frac{1}{1-z} \bullet\!\!-\!\!\circ\, \mathcal{H}(x) = \{ \cdots 0 \;\; 0 \;\; 0 \underset{x=0}{1} 1 \;\; 1 \cdots \}.$$

Integration of the DSS kernel given in Eq. 2.1 using $\blacktriangle_{even}$ is given by

$$T_{\blacktriangle_{even}}\left(x; \frac{k}{3}\right) \circ\!\!-\!\!\bullet\, T\left(z; \frac{k}{3}\right) \cdot \blacktriangle_{even,z},$$

where, e.g. in the case $k = 1$,

$$T_{\blacktriangle_{even}}\left(x; \frac{1}{3}\right) \circ\!\!-\!\!\bullet \left(\frac{1}{6}z^{-1} + \frac{2}{3} + \frac{1}{6}z\right) \cdot \frac{1}{1-z} = \frac{1}{6}\left(-1 + \frac{1}{z} + \frac{6}{1-z}\right)$$
$$\bullet\!\!-\!\!\circ\, -\frac{1}{6}\delta(x) + \frac{1}{6}\delta(x+1) + \mathcal{H}(x),$$

which corresponds to

x	$\cdots, -3, -2$	-1	0	1	$2, 3, \cdots$
$\{T_{\blacktriangle_{even}}(x; \frac{1}{3})\}$	0	$\frac{1}{6}$	$\frac{5}{6}$	1	1

,

[2]Here we do not go into details of the inverse transform of a z-transformed function about which one can find a nice introduction e.g. in [14, Sec. 4]. However, it is useful to remember several pairs of inverse transform that are used often:

$$z^n \bullet\!\!-\!\!\circ\, \delta(x-n),$$
$$\frac{1}{1-z} \bullet\!\!-\!\!\circ\, \mathcal{H}(x), \quad \text{and}$$
$$\frac{1}{1+z} \bullet\!\!-\!\!\circ\, (-1)^x \mathcal{H}(x),$$

where $\delta(x)$ is the impulse function and $\mathcal{H}(x)$ is the Heaviside function.

i.e. $T_{\blacktriangle_{even}}\left(x;\frac{1}{3}\right)=\{\cdots\ 0\ \frac{1}{6}\ \frac{5}{6}\ 1\ \cdots\}$.

Analogously, $\blacktriangle_{odd,z}$ is given by

$$\blacktriangle_{odd,z}=(\triangle_{odd,z})^{-1}=\left(\frac{1}{2}z^{-1}-\frac{1}{2}z\right)^{-1},$$

and the inverse transform of $\blacktriangle_{odd,z}$ is

$$\blacktriangle_{odd,z}=\frac{2z}{1-z^2}=\left(\frac{1}{1-z}-\frac{1}{1+z}\right)$$
$$\bullet\!\!-\!\!\circ\ \mathcal{H}(x)-(-1)^x\mathcal{H}(x)=\{\cdots 0\ \ 0\ \ 0\ \underset{x=0}{0}\ 2\ \ 0\ \ 2\cdots\}.$$

Integration of the DSS kernel using $\blacktriangle_{odd}$ is given by

$$T_{\blacktriangle_{odd}}\left(x;\frac{k}{3}\right)\ \circ\!\!-\!\!\bullet\ T\left(z;\frac{k}{3}\right)\cdot\blacktriangle_{odd,z},$$

where, e.g. in the case $k=1$,

$$T_{\blacktriangle_{odd,z}}\left(x;\frac{1}{3}\right)\ \circ\!\!-\!\!\bullet\ \left(\frac{1}{6}z^{-1}+\frac{2}{3}+\frac{1}{6}z\right)\cdot\frac{2z}{1-z^2}=\frac{1}{3}\left(-1+\frac{3}{1-z}+\frac{-1}{1+z}\right)$$
$$\bullet\!\!-\!\!\circ\ -\frac{1}{3}\delta(x)+\mathcal{H}(x)-\frac{(-1)^x}{3}\mathcal{H}(x)$$

which corresponds to

x	$\cdots,-2,-1$	0	1	2	$3,4,\cdots$
$\{T_{\blacktriangle_{odd}}(x;\frac{1}{3})\}$	0	$\frac{1}{3}$	$\frac{4}{3}$	$\frac{2}{3}$	$\{\frac{4}{3}\ \frac{2}{3}\}$

,

i.e. $T_{\blacktriangle_{odd}}\left(x;\frac{1}{3}\right)=\{\cdots\ 0\ \frac{1}{3}\ \{\frac{4}{3}\ \frac{2}{3}\}\ \cdots\}$. The coefficients obtained from integration of the DSS kernel with large variance can be derived in the same way.

From the derivation of $T_{\blacktriangle_{even}}$ and $T_{\blacktriangle_{odd}}$ as explicated above, one can recognize that the coefficients of $T_{\blacktriangle_{even}}$ are different from those of $T_{\blacktriangle_{odd}}$. In the case that differentiation and integration are simultaneously applied to a discrete signal, the even(odd)-number-sized differencing operator must be paired with the even(odd)-number-sized integration operator such that

$$T_{\blacktriangle_{even,z}}(z;\cdot)\cdot\triangle_{even,z}=T(z;\cdot)\cdot\blacktriangle_{even,z}\cdot\triangle_{even,z}=T(z;\cdot)\ \bullet\!\!-\!\!\circ\ T(x;\cdot)\quad\text{and}$$
$$T_{\blacktriangle_{odd,z}}(z;\cdot)\cdot\triangle_{odd,z}=T(z;\cdot)\cdot\blacktriangle_{odd,z}\cdot\triangle_{odd,z}=T(z;\cdot)\ \bullet\!\!-\!\!\circ\ T(x;\cdot).$$

Otherwise, one can not expect a correct result since

$$T_{\blacktriangle_{even}}(z;\cdot)\cdot\triangle_{odd,z}\neq T_{\blacktriangle_{odd}}(z;\cdot)\cdot\triangle_{even,z}\neq T(z;\cdot).$$

In other words, when one executes discrete integration and discrete differentiation at the same time, it must be considered that $\blacktriangle_{even}$ ($\blacktriangle_{odd}$) is necessarily paired with $\triangle_{even}$ ($\triangle_{odd}$).

In Higher Dimensions

For a given higher dimensional DSS kernel $T(\vec{x};\cdot)$ ($\vec{x}=\{x_1,x_2,\cdots,x_N\}$) of the form in Eq. 2.2, the differencing kernel through application of $\triangle_{x_\alpha}$ is derived such that

$$T_{\triangle_{x_\alpha}}(\vec{x};\cdot)=T(x_1;\cdot)*T(x_2;\cdot)*\cdots*T_{\triangle}(x_\alpha;\cdot)\cdots*T(x_N;\cdot).$$

Applying $\triangle_{even,x}$ to $T(x,y;\frac{1}{3})$ results in

$$\begin{aligned}T_{\triangle_{even,x}}\left(x,y;\frac{1}{3}\right)&=T_{\triangle_{even}}\left(x;\frac{1}{3}\right)*T\left(y;\frac{1}{3}\right)\\&=\begin{pmatrix}\frac{1}{6}&\frac{1}{2}&\frac{-1}{2}&\frac{-1}{6}\end{pmatrix}_x*\begin{pmatrix}\frac{1}{6}&\frac{2}{3}&\frac{1}{6}\end{pmatrix}_y=\begin{pmatrix}\frac{1}{36}&\frac{1}{12}&\frac{-1}{12}&\frac{-1}{36}\\\frac{1}{9}&\frac{1}{3}&\frac{-1}{3}&\frac{-1}{9}\\\frac{1}{36}&\frac{1}{12}&\frac{-1}{12}&\frac{-1}{36}\end{pmatrix},\end{aligned}$$

while applying $\triangle_{odd,y}$ to $T(x,y;\frac{1}{3})$ yields

$$\begin{aligned}T_{\triangle_{odd,y}}\left(x,y;\frac{1}{3}\right)&=T\left(x;\frac{1}{3}\right)*T_{\triangle_{odd}}\left(y;\frac{1}{3}\right)\\&=\begin{pmatrix}\frac{1}{6}&\frac{2}{3}&\frac{1}{6}\end{pmatrix}_x*\begin{pmatrix}\frac{1}{12}&\frac{1}{3}&0&\frac{-1}{3}&\frac{-1}{12}\end{pmatrix}_y\\&=\begin{pmatrix}\frac{1}{72}&\frac{1}{18}&\frac{1}{72}\\\frac{1}{18}&\frac{2}{9}&\frac{1}{18}\\0&0&0\\\frac{-1}{18}&\frac{-2}{9}&\frac{-1}{18}\\\frac{-1}{72}&\frac{-1}{18}&\frac{-1}{72}\end{pmatrix}.\end{aligned}$$

Tab. 2.8 gives a graphical illustration of the 2-D DSS first-order differencing kernels (even-number-sized as well as odd-number-sized) of variance $\frac{5}{3}$, which can be compared with the 2-D SG first-order differencing kernels of the same variance.

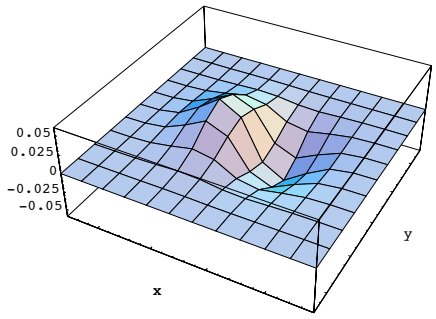	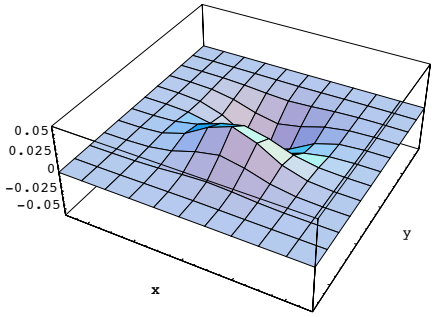
$T_{\triangle_{even,x}}(x, y; \frac{5}{3})$	$T_{\triangle_{even,y}}(x, y; \frac{5}{3})$
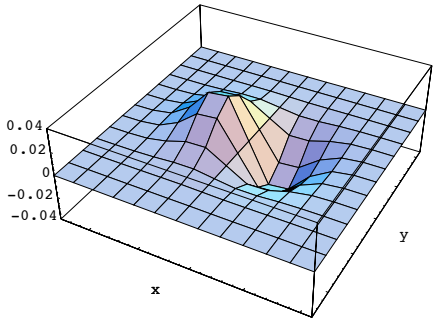	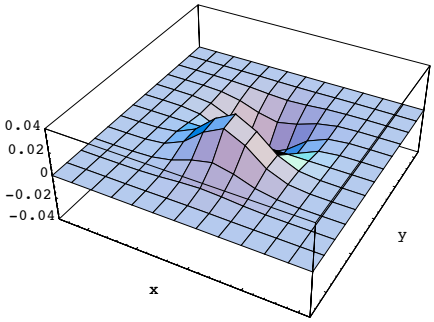
$T_{\triangle_{odd,x}}(x, y; \frac{5}{3})$	$T_{\triangle_{odd,y}}(x, y; \frac{5}{3})$
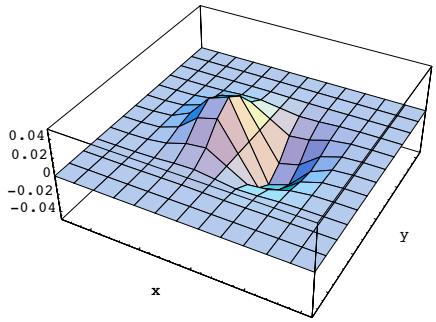	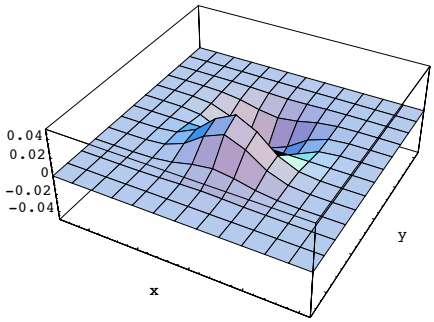
$SG_{\triangle_x}\left(x, y; \frac{5}{3}\right)$	$SG_{\triangle_y}\left(x, y; \frac{5}{3}\right)$

Table 2.8: Graphical illustration of the 2-D discrete first-order differencing kernels

3 Validation Criteria and Experimental Settings

We have derived an improved discrete scale-space formulation for 2-D and 3-D signals by supplementing the work of Lindeberg [13] (see [10] and [11]). In the previous section, the properties of the derived DSS kernel are thoroughly investigated compared with the sampled Gaussian which is commonly used in practice for approximating the continuous scale-space kernel.

The aim of this section is to validate the DSS kernel in comparison to the SG kernel under fairly practical conditions in order to characterize its performance with respect to smoothing and to differentiation. As important performance criteria, we consider the accuracy of approximation, the fulfillment of the non-enhancement requirement, and the accuracy of edge extraction. The first two criteria are related to the performance of smoothing, and the last criterion is related to the performance of differentiation. The last one is divided into two subcriteria, namely rotation invariance and steadiness from adjacency.

3.1 Accuracy of Approximation

We want to measure how accurately discrete convolution using the DSS kernel approximates the continuous convolution. To this end, we consider a continuous constant function $f(x) = c\,(x, c \in \mathbb{R})$. Theoretically, convolution of a constant function with the normalized Gaussian kernel results in the very constant function again

$$L(x;t) = f(x) * G(x;t) = c * G(x;t) = c. \tag{3.1}$$

This is explained by

$$c * \frac{1}{\sqrt{2\pi t}} e^{-\frac{x^2}{2t}} \circ\!\!-\!\!\bullet\; c\delta(\omega) \cdot e^{-\frac{\omega^2 \cdot t}{2}} = c\delta(\omega) \cdot e^{-\frac{0 \cdot t}{2}} = c\delta(\omega) \bullet\!\!-\!\!\circ\; c.$$

Convolution given in Eq. 3.1 is implemented practically by

$$L_d(x;t) = f_d(x) * G_d(x;t) = \{\cdots\ c\ \ c\ \ c\ \cdots\} * G_d(x;t), \tag{3.2}$$

where $f_d(x)$ is the constant discrete signal, $G_d(x;t)$ is the discrete scale-space kernel, and $L_d(x;t)$ is the scale-space representation resulting from *discrete convolution*.

As a simple example, by setting c e.g. to 100 for $f_d(x)$ of Eq. 3.2 with the large number of coefficients, we obtain the discrete scale-space representation of $T(x;t)$ and of $SG(x;t)$ e.g. with $t = \frac{2}{3}$

$$\begin{aligned} L_T\left(x;\frac{2}{3}\right) &= \{\cdots\ 100\ \ 100\ \ 100\ \ 100\ \ 100\ \cdots\} * \left\{\ \frac{1}{36}\ \ \frac{2}{9}\ \ \frac{1}{2}\ \ \frac{2}{9}\ \ \frac{1}{36}\ \right\} \\ &= \{\cdots\ 100\ \ 100\ \ 100\ \ 100\ \ 100\ \cdots\}, \\ L_{SG}\left(x;\frac{2}{3}\right) &= \{\cdots\ 100\ \ 100\ \ 100\ \ 100\ \ 100\ \cdots\} * \{\ 0.02433\ \ 0.23080\ \ 0.48860\ \ 0.23080\ \ 0.02433\ \} \\ &= \{\cdots\ 99.8854\ \ 99.8854\ \ 99.8854\ \ 99.8854\ \ 99.8854\ \cdots\}. \end{aligned}$$

Along t, in the same way, one can obtain $L_T(x;t)$ and $L_{SG}(x;t)$.

The approximation error of discrete convolution is calculated by measuring the distance between $L_d(x_l;t)$ and $L(x_l;t)$ at $x = x_l$

$$\xi_l(t) = |L_d(x_l;t) - L(x_l;t)|, \tag{3.3}$$

where $L_d(x_l;t)$ is from Eq. 3.2 and $L(x_l;t)$ is from Eq. 3.1. We consider here two indices, i.e. $\overline{\xi}$ and ξ_σ, which correspond to the *mean* and the *standard deviation* of $\xi(t)$ defined in Eq. 3.3 respectively, given by

$$\begin{aligned} \overline{\xi}(t) &= \frac{1}{(2n_l+1)} \sum_{l=-n_l}^{l=n_l} \xi_l(t), \\ \xi_\sigma(t) &= \sqrt{\frac{1}{(2n_l+1)} \sum_{l=-n_l}^{l=n_l} (\xi_l(t) - \overline{\xi}(t))^2}, \end{aligned} \tag{3.4}$$

where $2n_l + 1$ corresponds to the number of the coefficients of $L_d(x;\cdot)$.

The result of the approximation accuracy given by $< \overline{\xi}(t), \xi_\sigma(t) >$ is determined such that the smaller for a given t and the more consistent along t the approximation error is, the more accurate the approximation is.

3.2 Fulfillment of the Non-Enhancement Requirement

According to the prerequisites for the discrete scale-space formulation proposed by Lindeberg [13], a higher dimensional discrete scale-space kernel must obey the non-enhancement

requirement: If for some scale level t_0 a point x_0 has a local maximum (minimum) in the scale-space representation at that level (regarded as a function of the space coordinates only), then its value must not increase (decrease) when the scale parameter increases.

For a given synthetic (noiseless as well as weakly and strongly noisy[3]) image which has two local maxima and two local minima e.g. given by Fig. 3.1, we generate its scale-space representation resulting from convolving it with each discrete scale-space kernel (i.e. the DSS kernel and the SG kernel). Then, we observe if the intensity value of the local maxima (minima) of each scale-space representation does not increase (decrease) as the scale parameter gradually increases.

3.3 Accuracy of Edge Extraction

We intend to use the derived higher dimensional DSS first-order differencing kernels (i.e. $T_{\triangle_{even}}$ and $T_{\triangle_{odd}}$) described in Section 2.2 for higher dimensional edge extraction. For this, we examine the accuracy of the DSS differencing kernels compared with the SG differencing kernel for edge extraction.

For evaluating the result of edge extraction, we use a synthetic image in order to identify its edge image (we call it the *edge atlas*). The accuracy of $T_{\triangle_{even}}$, $T_{\triangle_{odd}}$, and $SG_{\triangle}$ for edge extraction is then assessed by measuring the error of extracted edges based on the edge atlas. Fig. 3.2 shows a synopsis of the procedure for evaluating the result of edge extraction. Given a synthetic image (its edge positions are known), on one hand, one can identify its edge atlas, from which the corresponding edge distance map that reflects the Euclidean distance from each edge position to any other pixel position of the edge atlas can be calculated. On the other hand, for the given synthetic image, one can vary the degree of edge width through Gaussian blurring and superposition of e.g. additive Gaussian noise in order to model a realistic blurred (i.e. sigmoid) edge with and without noise. Then the edge extractors using $T_{\triangle_{even}}$, $T_{\triangle_{odd}}$, and $SG_{\triangle}$ are applied to the blurred noisy image, which result in the extracted edge image. Note that we assume to know a priori the optimal

[3]Using additive Gaussian noise, we control the level of noise for a given synthetic image.

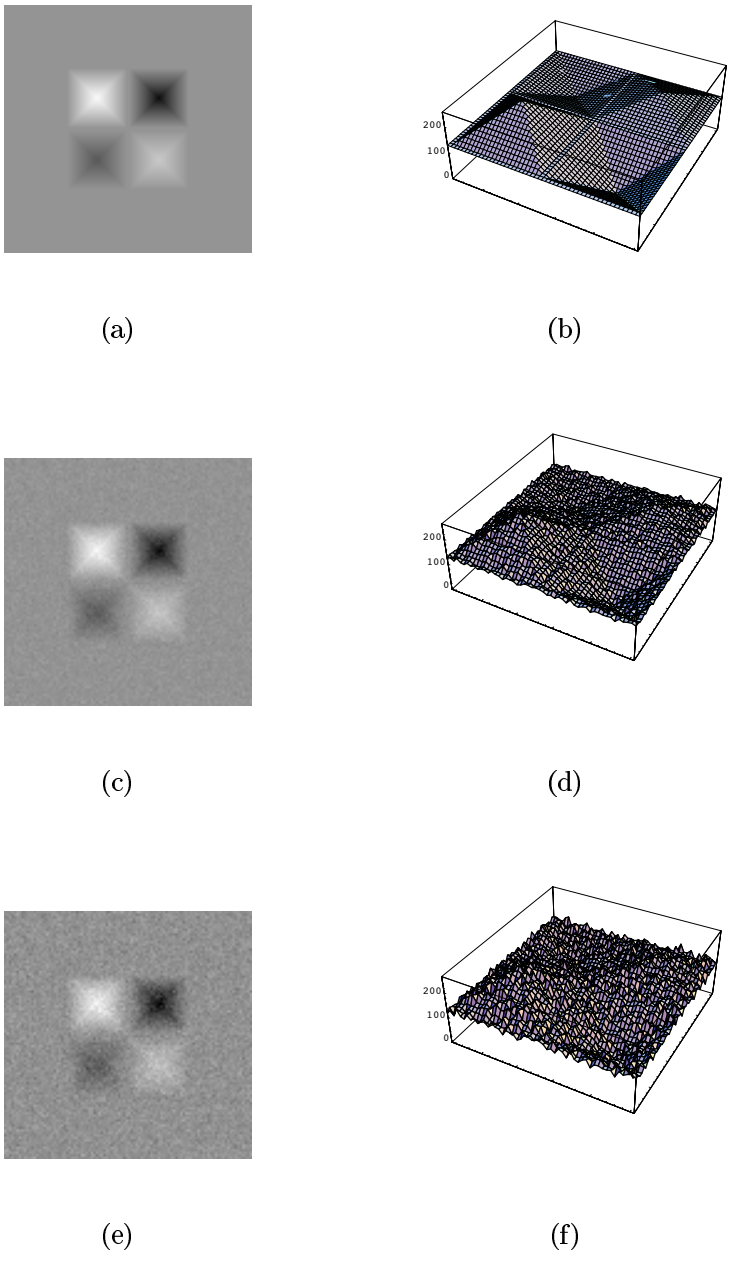

Figure 3.1: A synthetic image having two local maxima and two local minima; the one local maximum (minimum) has a high intensity value, whereas the other has a low intensity value. Noiseless image ((a)) and noisy images with the additive Gaussian noise ($\sigma = 5.0$ for (b) and $\sigma = 10.0$ for (c)) are shown in the left column, and the corresponding intensity profiles are given in the right column.

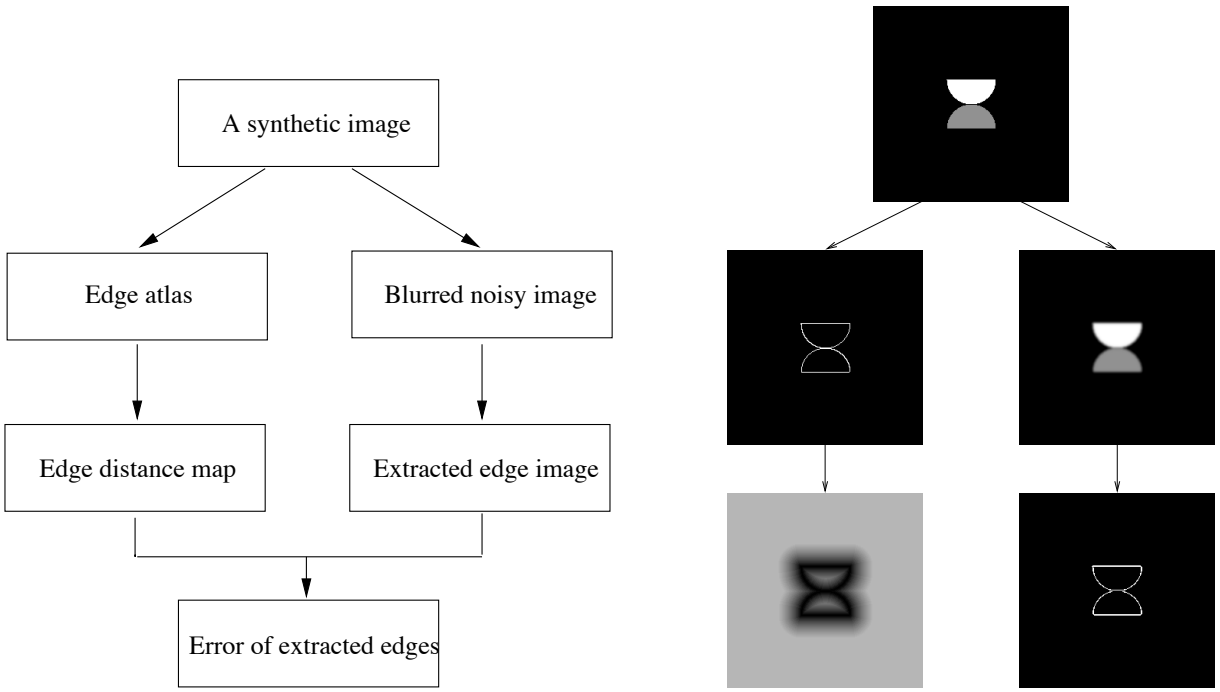

(a) Measuring error of extracted edges

(b) An example with a synthetic image

Figure 3.2: Synopsis of evaluating the result of edge extraction

scale value of the edge extractor since the edge width (i.e. the optimal scale of edge) is controlled in our experiment. This assumption is important since one can only expect a correct result of edge extraction by applying the optimal scale value to edge extraction. The accuracy of each discrete differencing kernel for edge extraction is then determined by the residual difference in global terms through masking the extracted edge image with the edge distance map.

In concrete terms, we denote $P_{l,\text{edge-atlas}}$ and $P_{l,\text{extracted-edge}}$ $(l = 1, \cdots, n_l)$ as the edge positions of the edge atlas and those of the extracted edge image, respectively, where n_l corresponds to the total number of edge positions. We consider three indices for measuring

the error of edge extraction in global terms given by

$$\overline{\psi} = \frac{1}{n_l}\sum_{l=1}^{n_l}\psi_l,$$

$$\psi_\sigma = \sqrt{\frac{1}{n_l}\sum_{l=1}^{n_l}(\psi_l - \overline{\psi})^2}, \quad \text{and} \tag{3.5}$$

$$\psi_{\max} = \max_{1\le l\le n_l}\psi_l,$$

where $\psi_l = ||P_{l,\text{edge-atlas}} - P_{l,\text{extracted-edge}}||$.

For the purpose of assessing the accuracy of each discrete differencing kernel used for edge extraction, we evaluate the result of edge extraction both qualitatively and quantitatively:

- From the viewpoint of a qualitative evaluation, we consider *rotation invariance* and *steadiness from adjacency* of each discrete differencing kernel for edge extraction.

- For a quantitative comparison of the accuracy result, we carry out the experiment with three different degrees of edge width (t_E=3, 7, and 13) and with three different levels of noise (n_0: noiseless, n_5: additive Gaussian noise of $\sigma = 5.0$, and n_{10}: additive Gaussian noise of $\sigma = 10.0$). As a consequence, the accuracy result of the form $< \overline{\psi}, \psi_\sigma, \psi_{\max} >$ for each discrete differencing kernel is compared under different degrees of edge width and different levels of noise.

Rotation Invariance

We have theoretically proven in [10] [11] that the derived 2-D and 3-D DSS kernels are rotationally least asymmetric. Now, we are interested in the matter whether $T_{\triangle_{even}}$ and $T_{\triangle_{odd}}$ as well as $SG_\triangle$ used for edge extraction are rotationally invariant.

We examine how consistent the edge extraction result of each discrete differencing kernel is under gradual rotation of an edge line. For this, we provide a series of ten synthetic images shown in Fig. 3.3 in which a straight edge line gradually rotates.

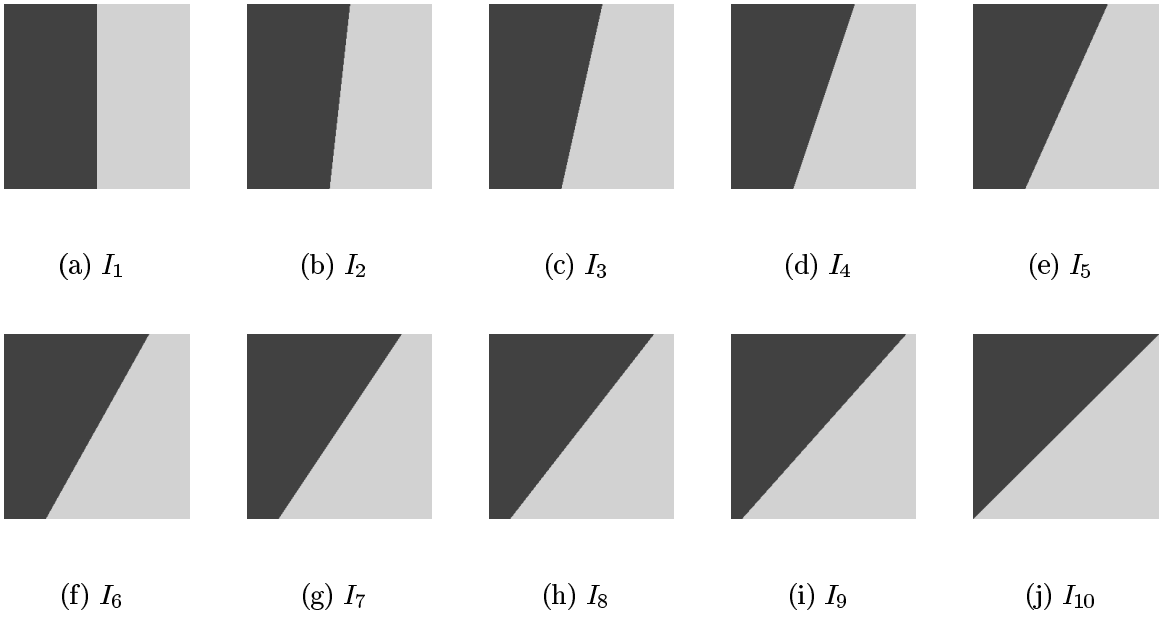

(a) I_1 (b) I_2 (c) I_3 (d) I_4 (e) I_5

(f) I_6 (g) I_7 (h) I_8 (i) I_9 (j) I_{10}

Figure 3.3: A series of ten synthetic images: A straight edge line gradually rotates.

For the given ten synthetic images in Fig. 3.3, a medium degree of edge width ($t_E = 7$) is given and three levels of noise (n_0, n_5, and n_{10}) are superimposed on each image. Then, we follow the procedure for evaluation of the edge extraction result described in Fig. 3.2, from which we obtain the error measurement of edge extraction (i.e. $< \overline{\psi}, \psi_\sigma, \psi_{\max} >$) of each discrete differencing kernel. Consequently, the error measurement of each discrete differencing kernel is compared from I_1 to I_{10} with respect to rotation invariance; the more consistent the results of the error measurement from I_1 to I_{10} are, the better the result with respect to rotational invariance is.

Steadiness from Adjacency

Though linear smoothing using a rotationally symmetric scale-space kernel greatly reduces the effect of random noise, it can also smooth across edges, which may cause an inaccurate result of edge extraction. In case of isolated edge structures, this problem can be coped with using optimal scale selection based on linear multiscale analysis (see for the details [12, Sec. 5]). However, when we intend to extract edges based on the linear scale-space

(a) SE1 (b) SE4 (c) CE1 (d) CE4

Figure 3.4: Four synthetic images having closely adjacent edge structures

approach (even using optimal scale selection) from a higher dimensional image ($n \geq 2$) that contains closely adjacent highly curved edge structures, we can hardly expect an accurate result of edge extraction. A typical example of such edge structure is a corner. For a given corner, smoothing its curve may result in a displacement or a disappearance of prominent structures after smoothing, since adjacent edges are blended with one another through smoothing (see e.g. for the problem of corners [16]). This is one of the intrinsic problems of higher dimensional edge extraction.

We do not attempt here to solve this general problem, but we are to examine the steadiness of each discrete differencing kernel for edge extraction applied to an image that contains closely adjacent edge structures. For that, as shown in Fig. 3.4, we provide four synthetic images. In Fig. 3.4, SE1 and SE4 contain two intersecting straight edge lines forming two L-corners (where one has high contrast and the other low contrast in intensity) such as to place their apexes at each other. The between-angle of L-corners in SE1 is wide, whereas that of L-corners in SE4 is narrow. CE1 and CE4 contain two intersecting circular edge contours, where the radius in CE1 is larger than that in CE4. Except for the edge type, CE1 and CE4 are analogous to SE1 and SE4.

For the four synthetic images given in Fig. 3.4, three different degrees of edge width ($t_E = 3, 7$, and 13) are given (see Fig 3.5), on which three levels of noise (n_0, n_5, and n_{10}) are superimposed. Then, similarly to the experiment for rotation invariance, we follow the procedure for evaluation of the edge extraction result described in Fig. 3.2, from which we

obtain the error measurement of edge extraction (i.e. $< \overline{\psi}, \psi_\sigma, \psi_{\max} >$) of each discrete differencing kernel.

As a consequence, with respect to steadiness from adjacency, the results of edge extraction by each discrete differencing kernel are compared under different degrees of edge width and different levels of noise. The obtained results are compared not only for each image but also among four different image types.

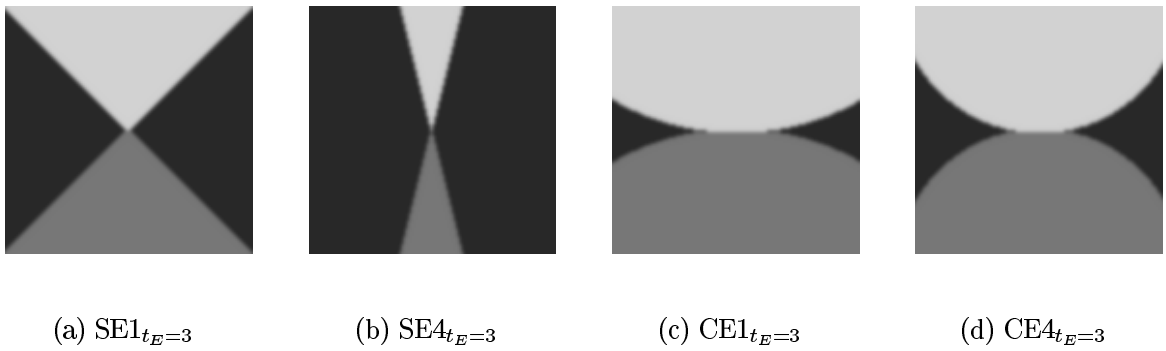

(a) SE1$_{t_E=3}$ (b) SE4$_{t_E=3}$ (c) CE1$_{t_E=3}$ (d) CE4$_{t_E=3}$

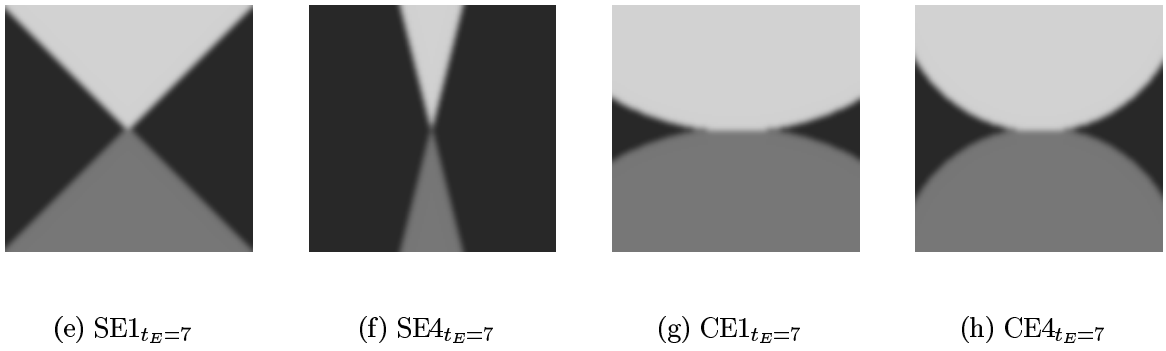

(e) SE1$_{t_E=7}$ (f) SE4$_{t_E=7}$ (g) CE1$_{t_E=7}$ (h) CE4$_{t_E=7}$

(i) SE1$_{t_E=13}$ (j) SE4$_{t_E=13}$ (k) CE1$_{t_E=13}$ (l) CE4$_{t_E=13}$

Figure 3.5: Blurring of four synthetic images in Fig. 3.4 in three levels: In the first, the middle, and the last row, the images are blurred for a small ($t_E = 3$), a middle ($t_E = 7$), and a large ($t_E = 13$) edge width, respectively.

4 Result of the Validation and Assessment

In this section, we present the results of our validation study from the previous section. A brief summary is given at the last subsection.

4.1 Accuracy of Approximation

The result of approximation accuracy is given both for the DSS kernel and for the SG kernel in Tab. 4.1, where the values of $< \overline{\xi}(t), \xi_\sigma(t) >$ are derived from the equations defined in Eq. 3.4.

From Tab. 4.1, one can see that $\overline{\xi}_T(t)$ gives zero consistently as t gradually increases, which implies that discrete convolution with $T(x;t)$ accurately approximates continuous convolution for any t. However, $\overline{\xi}_{SG}(t)$ inconsistently varies with t, even attains a maximum at a small t. This shows that $SG(x;t)$ is not superior to $T(x;t)$ with respect to the approximation of discrete convolution when t gets smaller. The undesirable result of the SG kernel is connected with the analysis result of the SG kernel in [9, Sec.4], where it was shown that the SG kernel is not normalized to one and that this fact gets worse as the scale parameter decreases (note that the derived DSS kernel is normalized to one at any t).

4.2 Fulfillment of the Non-Enhancement Requirement

Tab. 4.2 and Tab. 4.3 show the intensity values of the two local maxima and two local minima of the scale-space representation (by $T(x,y;t)$ and $SG(x,y;t)$, respectively) of Fig. 3.1(a), as t gradually increases. Tab. 4.4 and Tab. 4.5 present those of Fig. 3.1(c), and Tab. 4.6 and Tab. 4.7 give those of Fig. 3.1(e). Furthermore, Fig. 4.1 and Fig. 4.2 depict the development of two local maxima, while Fig. 4.3 and Fig. 4.4 illustrate the development of two local minima, where each row differs in the level of noise and each column differs in the applied discrete scale-space kernel.

From the values obtained in Tab. 4.2 - Tab. 4.5 as well as in Fig. 4.1 - Fig. 4.4, one

	$T(x;t)$		$SG(x;t)$	
t	$\overline{\xi}(t)$	$\xi_\sigma(t)$	$\overline{\xi}(t)$	$\xi_\sigma(t)$
$\frac{1}{3}$	0.0	0.0	0.0651041	0.0
$\frac{2}{3}$	0.0	0.0	0.114635	0.0
$\frac{3}{3}$	0.0	0.0	0.0270641	0.0
$\frac{4}{3}$	0.0	0.0	0.0059563	0.0
$\frac{5}{3}$	0.0	0.0	0.00128657	0.0
$\frac{6}{3}$	0.0	0.0	0.000276412	0.0
$\frac{7}{3}$	0.0	0.0	0.0000593371	0.0
$\frac{8}{3}$	0.0	0.0	0.0000127495	0.0
$\frac{9}{3}$	0.0	0.0	2.74371×10^{-6}	0.0
$\frac{10}{3}$	0.0	0.0	5.91491×10^{-7}	0.0
$\frac{11}{3}$	0.0	0.0	1.2774×10^{-7}	0.0
$\frac{12}{3}$	0.0	0.0	2.76339×10^{-8}	0.0

(a) $< \overline{\xi}(t), \xi_\sigma(t) >_T$ vs. $< \overline{\xi}(t), \xi_\sigma(t) >_{SG}$

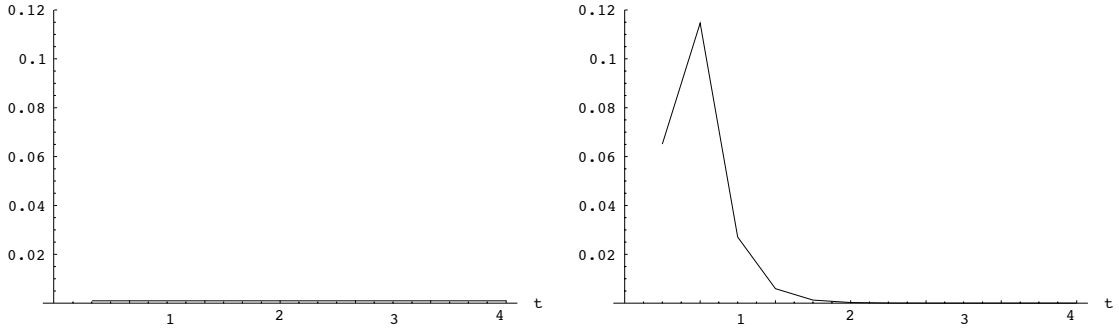

$\overline{\xi}_T(t)$ $\overline{\xi}_{SG}(t)$

(b) Graphical illustration of $\overline{\xi}(t)$ along t

Table 4.1: The accuracy of approximation of the DSS kernel compared with the SG kernel.

can see clearly that the intensity values of the local maxima (minima) in the scale-space representation generated by both $T(x, y; t)$ and $SG(x, y; t)$ do not increase (decrease) as the scale parameter increases. The level of noise and the intensity contrast can influence the shape of covergency of local extrema, however, they do not affect the principal non-enhancement behavior of the local extrema.

Based on this result, as a consequence, it can be said that the DSS kernel as well as the SG kernel fulfill the non-enhancement requirement.

4.3 Accuracy of Edge Extraction

For higher dimensional edge extraction, we employ the non-maximum suppression method ([3]), in which a maximum of the gradient magnitude in the gradient direction is defined as an edge point. It is noticeable that the local maxima approach using the gradient operator (e.g. the non-maximum suppression) has advantages compared with the zero-crossing approach based on the second-order derivative (e.g. the Laplacian operator) in several respects (see for details [12, Sec. 4.1]). The accuracy of edge extraction is given by the form defined in Eq. 3.5.

Rotation Invariance

With respect to rotation invariance of the discrete first-order differencing kernel for edge extraction, the results of edge extraction using $T_{\triangle_{even}}$, $T_{\triangle_{odd}}$, and $SG_{\triangle}$ are given in Tab. 4.8 - Tab. 4.10, where each table differs in the level of noise added to the images of Fig. 3.3. Rotation invariance of each discrete first-order differencing kernel is determined by comparison of the accuracy result of edge extraction from I_1 to I_{10}.

In Tab. 4.8 - Tab. 4.10, one can notice a few interesting aspects. First, the error of edge extraction using $T_{\triangle_{even}}$ is higher than that using $T_{\triangle_{odd}}$ and $SG_{\triangle}$ for a given image. Second, the edge extraction error using $T_{\triangle_{odd}}$ is almost identical with that using $SG_{\triangle}$. Moreover, the accuracy result of edge extraction using $T_{\triangle_{even}}$ from I_1 to I_{10} is rather inconsistent compared with that using $T_{\triangle_{odd}}$ and $SG_{\triangle}$, which definitely appears in the case of the

t	Local Maxima		Local Minima	
0	$f_{n_0}(37,37)=250$	$f_{n_0}(62,62)=190$	$f_{n_0}(62,37)=10$	$f_{n_0}(37,62)=70$
$\frac{1}{3}$	244.444443	187.222214	15.555555	72.777786
$\frac{2}{3}$	241.419739	185.709869	18.580248	74.290123
$\frac{3}{3}$	239.212967	184.606476	20.787035	75.393509
$\frac{4}{3}$	237.393402	183.696716	22.606596	76.303291
$\frac{5}{3}$	235.807480	182.903763	24.192522	77.096260
$\frac{6}{3}$	234.382553	182.191284	25.617418	77.808708
$\frac{7}{3}$	233.077576	181.538773	26.922403	78.461197
$\frac{8}{3}$	231.866501	180.933228	28.133535	79.066757
$\frac{9}{3}$	230.731400	180.365707	29.268585	79.634300
$\frac{10}{3}$	229.659683	179.829834	30.340332	80.170158
$\frac{11}{3}$	228.641693	179.320831	31.358320	80.679146
$\frac{12}{3}$	227.670044	178.835022	32.329922	81.164948
$\frac{13}{3}$	226.739044	178.369476	33.260941	81.630486
$\frac{14}{3}$	225.843872	177.921951	34.156101	82.078033
$\frac{15}{3}$	224.980774	177.490417	35.019234	82.509628
$\frac{16}{3}$	224.146393	177.073242	35.853554	82.926773
$\frac{17}{3}$	223.338226	176.669159	36.661774	83.330887
$\frac{18}{3}$	222.553802	176.276871	37.446201	83.723106
$\frac{19}{3}$	221.791183	175.895615	38.208820	84.104424
$\frac{20}{3}$	221.048660	175.524353	38.951336	84.475677

Table 4.2: $L_{T_{n_0}}(x,y;t) = f_{n_0}(x,y) * T(x,y;t)$; $f_{n_0}(x,y)$ corresponds to the noiseless image given in Fig. 3.1(a).

t	Local Maxima		Local Minima	
0	$f(37,37)=250$	$f(62,62)=190$	$f(62,37)=10$	$f(37,62)=70$
$\frac{1}{3}$	244.462250	187.146515	15.199319	72.515053
$\frac{2}{3}$	240.889160	185.295624	18.515106	74.108620
$\frac{3}{3}$	239.085480	184.507538	20.773817	75.351730
$\frac{4}{3}$	237.361969	183.673248	22.607061	76.295784
$\frac{5}{3}$	235.797638	182.897171	24.195652	77.096146
$\frac{6}{3}$	234.378067	182.188660	25.620512	77.809875
$\frac{7}{3}$	233.074707	181.537277	26.924995	78.462410
$\frac{8}{3}$	231.864288	180.932144	28.135654	79.067810
$\frac{9}{3}$	230.729645	180.364838	29.270342	79.635162
$\frac{10}{3}$	229.658188	179.829071	30.341805	80.170883
$\frac{11}{3}$	228.640411	179.320236	31.359581	80.679787
$\frac{12}{3}$	227.668945	178.834503	32.331009	81.165512
$\frac{13}{3}$	226.738113	178.368988	33.261909	81.630943
$\frac{14}{3}$	225.843063	177.921555	34.156948	82.078484
$\frac{15}{3}$	224.980026	177.490005	35.020000	82.509979
$\frac{16}{3}$	224.145782	177.072861	35.854252	82.927116
$\frac{17}{3}$	223.337601	176.668762	36.662399	83.331207
$\frac{18}{3}$	222.553223	176.276627	37.446774	83.723351
$\frac{19}{3}$	221.790619	175.895309	38.209339	84.104660
$\frac{20}{3}$	221.048218	175.524109	38.951813	84.475899

Table 4.3: $L_{SG_{n0}}(x,y;t) = f_{n_0}(x,y) * SG(x,y;t)$; $f_{n_0}(x,y)$ corresponds to the noiseless image given in Fig. 3.1(a).

t	Local Maxima		Local Minima	
0	$f_{n_5}(37,37) = 254.16$	$f_{n_5}(61,62) = 191.18$	$f_{n_5}(62,37) = 7.99$	$f_{n_5}(37,62) = 73.90$
$\frac{1}{3}$	245.086807	186.923248	13.758581	75.197769
$\frac{2}{3}$	240.912704	184.650742	17.198782	76.427933
$\frac{3}{3}$	238.333588	183.183289	19.738026	77.411713
$\frac{4}{3}$	236.421066	182.108902	21.803780	78.219063
$\frac{5}{3}$	234.845352	181.252411	23.569942	78.905586
$\frac{6}{3}$	233.468185	180.528839	25.127234	79.507935
$\frac{7}{3}$	232.223480	179.893219	26.530285	80.050873
$\frac{8}{3}$	231.075562	179.319794	27.814705	80.551163
$\frac{9}{3}$	230.002945	178.792755	29.004961	81.020157
$\frac{10}{3}$	228.991409	178.301773	30.118534	81.465508
$\frac{11}{3}$	228.030807	177.839722	31.168339	81.892456
$\frac{12}{3}$	227.113525	177.401459	32.164173	82.304420
$\frac{13}{3}$	226.233658	176.983078	33.113667	82.703873
$\frac{14}{3}$	225.386597	176.581635	34.022861	83.092453
$\frac{15}{3}$	224.568481	176.194824	34.896633	83.471420
$\frac{16}{3}$	223.776154	175.820831	35.738983	83.841576
$\frac{17}{3}$	223.007141	175.458237	36.553204	84.203613
$\frac{18}{3}$	222.259155	175.105774	37.342091	84.558060
$\frac{19}{3}$	221.530411	174.762482	38.107986	84.905312
$\frac{20}{3}$	220.819275	174.427505	38.852882	85.245743

Table 4.4: $L_{T_{n_5}}(x,y;t) = f_{n_5}(x,y) * T(x,y;t)$; $f_{n_5}(x,y)$ corresponds to the image with weak noise given in Fig. 3.1(c).

t	Local Maxima		Local Minima	
0	$f_{n_5}(37,37) = 254.16$	$f_{n_5}(61,62) = 191.18$	$f_{n_5}(62,37) = 7.99$	$f_{n_5}(37,62) = 73.90$
$\frac{1}{3}$	245.317810	186.957428	13.357513	74.995941
$\frac{2}{3}$	240.305496	184.193634	17.176044	76.232742
$\frac{3}{3}$	238.160995	183.044586	19.758074	77.364235
$\frac{4}{3}$	236.370392	182.053009	21.820951	78.209236
$\frac{5}{3}$	234.828018	181.223816	23.581570	78.905151
$\frac{6}{3}$	233.460892	180.512177	25.135174	79.509666
$\frac{7}{3}$	232.219650	179.882889	26.536026	80.052704
$\frac{8}{3}$	231.073151	179.313034	27.819101	80.552612
$\frac{9}{3}$	230.001175	178.788177	29.008478	81.021172
$\frac{10}{3}$	228.989990	178.298538	30.121424	81.466179
$\frac{11}{3}$	228.029526	177.837341	31.170757	81.892822
$\frac{12}{3}$	227.112473	177.399658	32.166225	82.304596
$\frac{13}{3}$	226.232742	176.981659	33.115417	82.703926
$\frac{14}{3}$	225.385742	176.580490	34.024372	83.092422
$\frac{15}{3}$	224.567749	176.193954	34.897949	83.471329
$\frac{16}{3}$	223.775497	175.820114	35.740128	83.841454
$\frac{17}{3}$	223.006500	175.457626	36.554214	84.203499
$\frac{18}{3}$	222.258636	175.105286	37.342968	84.557938
$\frac{19}{3}$	221.529922	174.762039	38.108761	84.905205
$\frac{20}{3}$	220.818878	174.427185	38.853569	85.245651

Table 4.5: $L_{SG_{n_5}}(x,y;t) = f_{n_5}(x,y) * SG(x,y;t)$; $f_{n_5}(x,y)$ corresponds to the image with weak noise given in Fig. 3.1(c).

t	Local Maxima		Local Minima	
0	$f_{n10}(37,37) = 258.32$	$f_{n10}(58,62) = 197.66$	$f_{n10}(63,37) = 0.89$	$f_{n10}(33,63) = 54.60$
$\frac{1}{3}$	245.729187	179.939392	13.026099	72.709305
$\frac{2}{3}$	240.405655	173.912262	17.899435	79.438072
$\frac{3}{3}$	237.454224	171.601822	20.822224	82.753471
$\frac{4}{3}$	235.448776	170.598709	23.035704	84.721535
$\frac{5}{3}$	233.883240	170.096176	24.886374	86.030258
$\frac{6}{3}$	232.553787	169.797501	26.498781	86.970711
$\frac{7}{3}$	231.369339	169.584061	27.934372	87.688972
$\frac{8}{3}$	230.284653	169.405304	29.232155	88.266327
$\frac{9}{3}$	229.274490	169.238571	30.420275	88.750999
$\frac{10}{3}$	228.323166	169.073761	31.519979	89.172691
$\frac{11}{3}$	227.419891	168.906601	32.547585	89.550400
$\frac{12}{3}$	226.556946	168.735428	33.515682	89.896446
$\frac{13}{3}$	225.728271	168.559921	34.434052	90.219147
$\frac{14}{3}$	224.929291	168.380371	35.310349	90.524117
$\frac{15}{3}$	224.156174	168.197311	36.150562	90.815308
$\frac{16}{3}$	223.405899	168.011307	36.959476	91.095497
$\frac{17}{3}$	222.676025	167.822922	37.740940	91.366638
$\frac{18}{3}$	221.964493	167.632782	38.498055	91.630196
$\frac{19}{3}$	221.269608	167.441177	39.233372	91.887260
$\frac{20}{3}$	220.589905	167.248611	39.949017	92.138618

Table 4.6: $L_{T_{n10}}(x,y;t) = f_{n10}(x,y) * T(x,y;t)$; $f_{n10}(x,y)$ corresponds to the image with strong noise given in Fig. 3.1(e).

t	Local Maxima		Local Minima	
0	$f_{n_{10}}(37,37) = 258.32$	$f_{n_{10}}(58,62) = 197.66$	$f_{n_{10}}(63,37) = 0.89$	$f_{n_{10}}(33,63) = 54.60$
$\frac{1}{3}$	246.173416	180.804596	12.266218	71.532051
$\frac{2}{3}$	239.721863	173.093338	18.041285	79.535530
$\frac{3}{3}$	237.236496	171.243027	20.928852	82.894577
$\frac{4}{3}$	235.378784	170.442688	23.086308	84.811775
$\frac{5}{3}$	233.858337	170.022888	24.912437	86.085533
$\frac{6}{3}$	232.543732	169.759705	26.515219	87.005806
$\frac{7}{3}$	231.364609	169.562973	27.946579	87.712143
$\frac{8}{3}$	230.281998	169.392670	29.241974	88.282166
$\frac{9}{3}$	229.272705	169.230576	30.428352	88.762093
$\frac{10}{3}$	228.321762	169.068512	31.526642	89.180618
$\frac{11}{3}$	227.418686	168.903000	32.553051	89.556145
$\frac{12}{3}$	226.555908	168.732880	33.520149	89.900673
$\frac{13}{3}$	225.727356	168.558090	34.437698	90.222275
$\frac{14}{3}$	224.928467	168.378998	35.313320	90.526489
$\frac{15}{3}$	224.155472	168.196259	36.152985	90.817108
$\frac{16}{3}$	223.405273	168.010529	36.961468	91.096848
$\frac{17}{3}$	222.675461	167.822327	37.742565	91.367683
$\frac{18}{3}$	221.964066	167.632263	38.499393	91.631020
$\frac{19}{3}$	221.269196	167.440781	39.234497	91.887909
$\frac{20}{3}$	220.589630	167.248352	39.949944	92.139160

Table 4.7: $L_{SG_{n_{10}}}(x,y;t) = f_{n_{10}}(x,y) * SG(x,y;t)$; $f_{n_{10}}(x,y)$ corresponds to the image with strong noise given in Fig. 3.1(e).

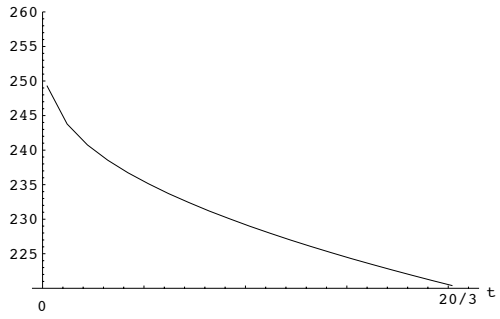

(a) $L_{T_{n_0}}$

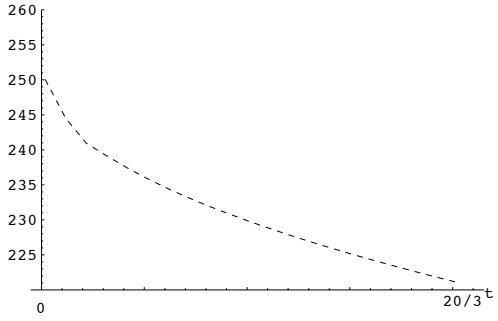

(b) $L_{SG_{n_0}}$

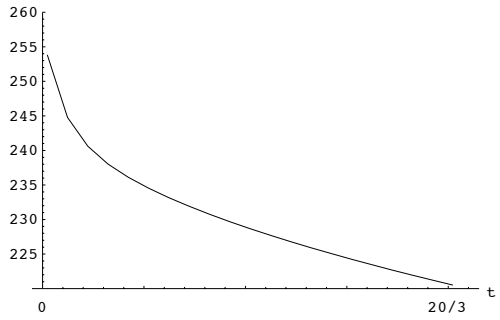

(c) $L_{T_{n_5}}$

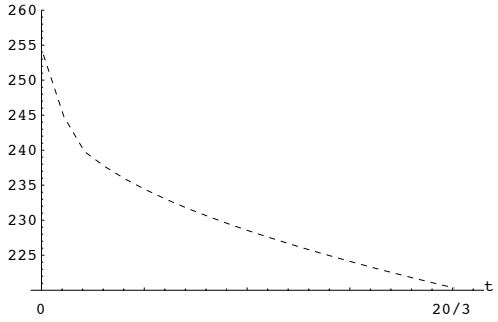

(d) $L_{SG_{n_5}}$

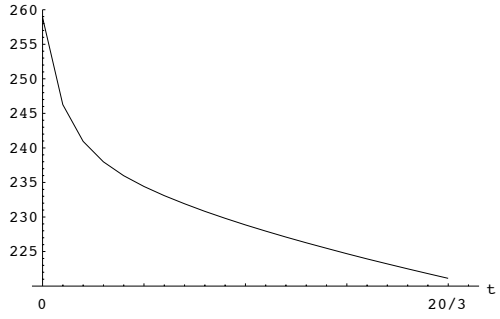

(e) $L_{T_{n_{10}}}$

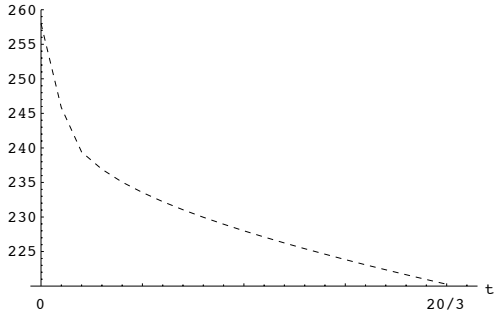

(f) $L_{SG_{n_{10}}}$

Figure 4.1: Development of the local maxima with a high intensity contrast along t.

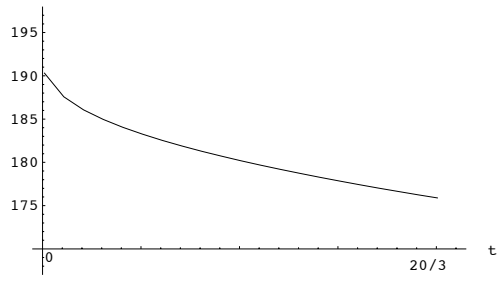

(a) $L_{T_{n_0}}$

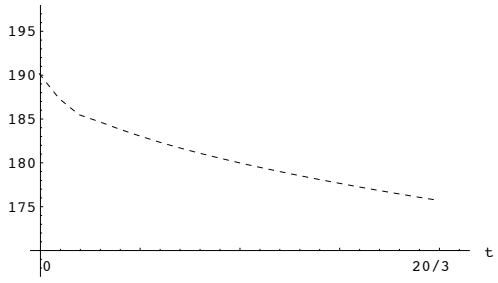

(b) $L_{SG_{n_0}}$

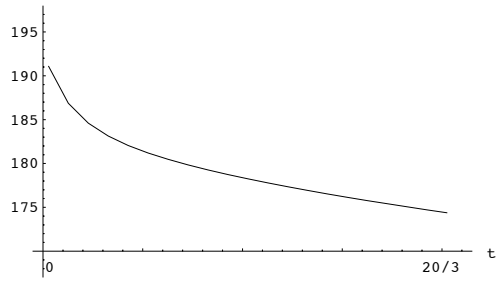

(c) $L_{T_{n_5}}$

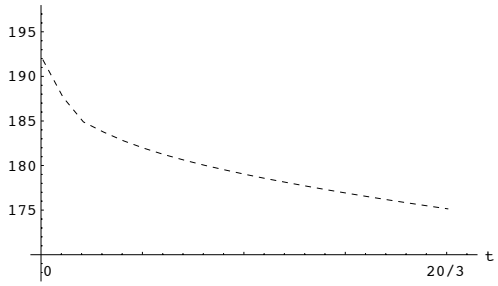

(d) $L_{SG_{n_5}}$

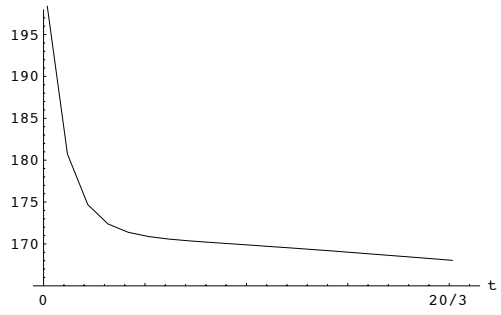

(e) $L_{T_{n_{10}}}$

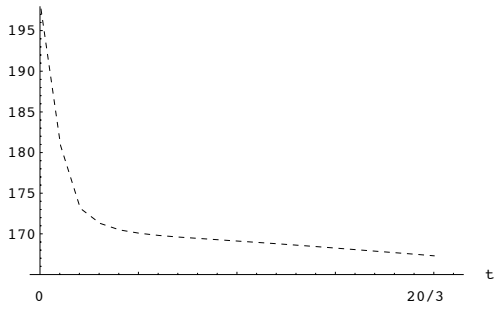

(f) $L_{SG_{n_{10}}}$

Figure 4.2: Development of the local maximum with a low intensity contrast along t.

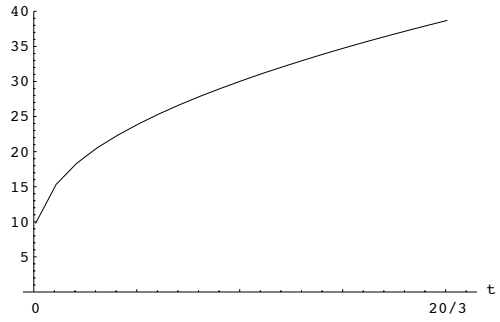

(a) $L_{T_{n_0}}$

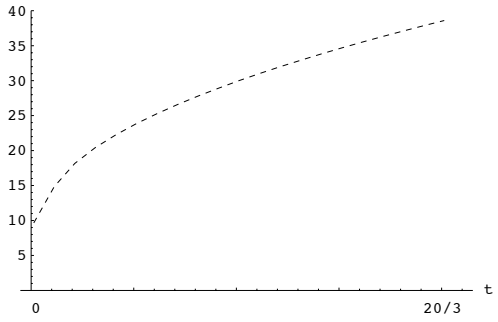

(b) $L_{SG_{n_0}}$

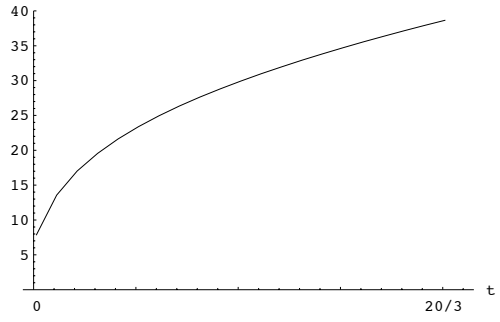

(c) $L_{T_{n_5}}$

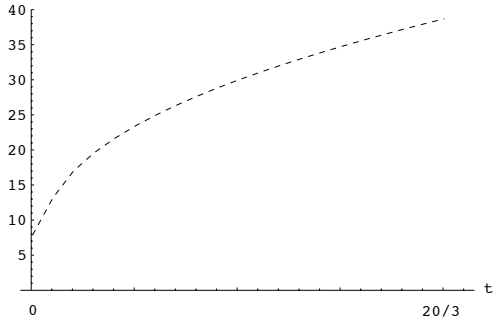

(d) $L_{SG_{n_5}}$

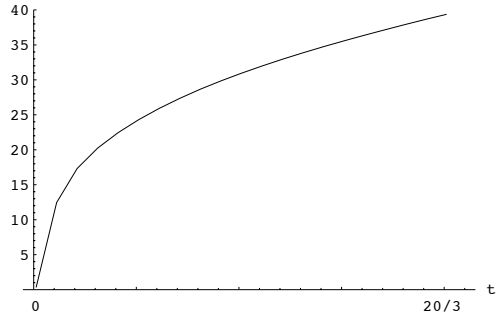

(e) $L_{T_{n_{10}}}$

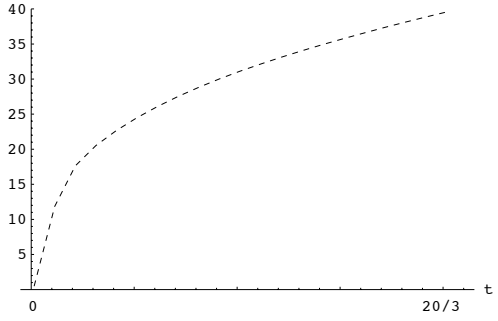

(f) $L_{SG_{n_{10}}}$

Figure 4.3: Development of the local minimum with a high intensity contrast along t.

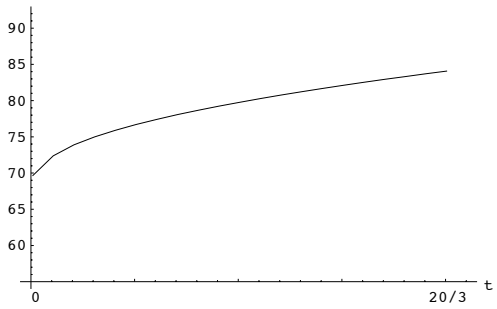

(a) $L_{T_{n_0}}$

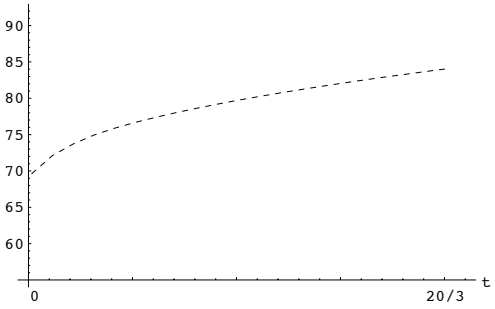

(b) $L_{SG_{n_0}}$

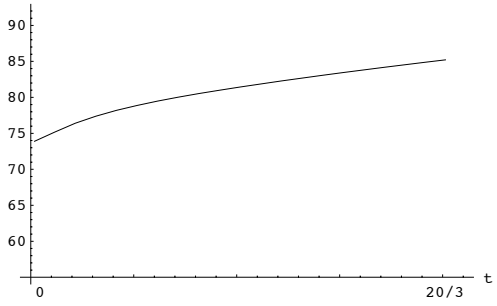

(c) $L_{T_{n_5}}$

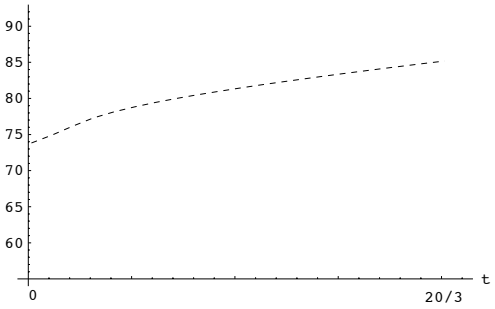

(d) $L_{SG_{n_5}}$

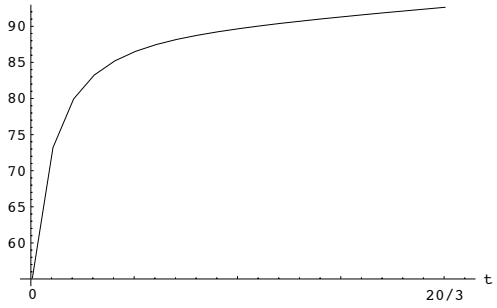

(e) $L_{T_{n_{10}}}$

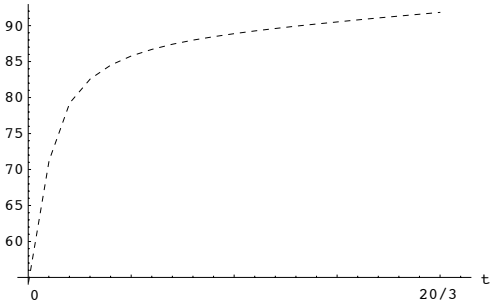

(f) $L_{SG_{n_{10}}}$

Figure 4.4: Development of the local minimum with a low intensity contrast along t.

noiseless images in Tab. 4.8. This shows that $T_{\triangle_{even}}$ is inferior to both $T_{\triangle_{odd}}$ and $SG_{\triangle}$ with respect to rotation invariance for edge extraction. However, as seen in Tab. 4.10, in the case of a strongly noisy image, one can hardly find a remarkable difference of the edge extraction results using $T_{\triangle_{even}}$, $T_{\triangle_{odd}}$, and $SG_{\triangle}$.

Steadiness from Adjacency

Regarding steadiness from adjacency of the discrete first-order differencing kernel for edge extraction, the results of edge extraction using $T_{\triangle_{even}}$, $T_{\triangle_{odd}}$, and $SG_{\triangle}$ are given in Tab. 4.11 - Tab. 4.14, where each table differs in the type of the applied images (i.e. Tab. 4.11 is for Fig. 3.4(a), Tab. 4.12 for Fig. 3.4(b), Tab. 4.13 for Fig. 3.4(c), and Tab. 4.14 for Fig. 3.4(d)). Complementarity, Fig 4.5 presents the graphical illustrations of the edge extraction result based on the classification of $\overline{\psi}$ by three different types of the discrete first-order differencing kernel and by three levels of noise. Fig 4.5 gives a nice graphical comparison of the results from four different image types for a given discrete first-order differencing kernel under certain level of noise.

One can find three conspicuous common aspects in Tab. 4.11 - Tab. 4.14. First, for a given image, $\overline{\psi}_{T_{\triangle_{even}}}$ is much larger than $\overline{\psi}_{T_{\triangle_{odd}}}$ and $\overline{\psi}_{SG_{\triangle}}$. Second, in the case of the small edge width under strong noise, $T_{\triangle_{odd}}$ obviously performs better than $SG_{\triangle}$. Besides it, the values of $\overline{\psi}_{T_{\triangle_{odd}}}$ are similar to those of $\overline{\psi}_{SG_{\triangle}}$ on the whole. The third, except for the case of strong noise (i.e. n_{10} in our experiment), the result of edge extraction is hardly influenced by the degree of edge width. On the other hand, one can observe several considerable phenomena from Fig. 4.5. First, regardless of the level of noise, of the edge width, and of the used discrete differencing kernel, SE1 is the steadiest image type of the adjacent edge structure in edge extraction (i.e. $\overline{\psi}_{SE1}$ is the smallest) and CE4 is the second steadiest one. Moreover, the between-gap of the edge extraction errors derived from four different image types using $T_{\triangle_{even}}$ is much wider than that using $\overline{\psi}_{T_{\triangle_{odd}}}$ and $\overline{\psi}_{SG_{\triangle}}$. In particular, the edge extraction results using $T_{\triangle_{even}}$ applied to SE4 and to CE1 are relatively poor (see Fig. 4.5[(a), (d), (g)]).

	$T_{\triangle_{even}}$			$T_{\triangle_{odd}}$			$SG_{\triangle}$		
	$\overline{\psi}$	ψ_σ	$\psi_{\max}$	$\overline{\psi}$	ψ_σ	$\psi_{\max}$	$\overline{\psi}$	ψ_σ	$\psi_{\max}$
$I_{1_{n_0}}$	1.00	0.00	1.00	0.50	0.50	1.00	0.50	0.50	1.00
$I_{2_{n_0}}$	1.00	0.00	1.00	0.51	0.50	1.00	0.51	0.50	1.00
$I_{3_{n_0}}$	1.00	0.00	1.00	0.51	0.50	1.00	0.51	0.50	1.00
$I_{4_{n_0}}$	1.00	0.00	1.00	0.50	0.50	1.00	0.50	0.50	1.00
$I_{5_{n_0}}$	0.90	0.30	1.00	0.50	0.50	1.00	0.50	0.50	1.00
$I_{6_{n_0}}$	0.94	0.33	1.41	0.50	0.50	1.00	0.50	0.50	1.00
$I_{7_{n_0}}$	0.75	0.43	1.00	0.50	0.50	1.00	0.50	0.50	1.00
$I_{8_{n_0}}$	0.91	0.42	1.41	0.50	0.50	1.00	0.50	0.50	1.00
$I_{9_{n_0}}$	0.95	0.34	2.00	0.50	0.50	1.00	0.50	0.50	1.00
$I_{10_{n_0}}$	1.00	0.00	1.00	0.50	0.50	1.00	0.50	0.50	1.00

(a) Errors of extracted edges.

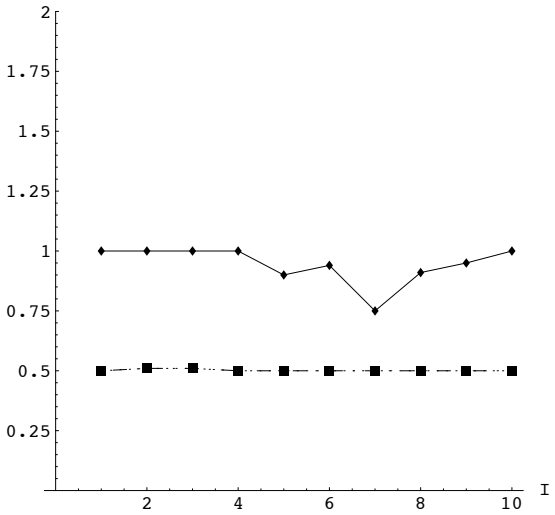

(b) Graphical illustration of $\overline{\psi}$ from $I_{1_{n_0}}$ to $I_{10_{n_0}}$.
(—◆— : $\overline{\psi}_{T_{\triangle_{even}}}$, ···★··· : $\overline{\psi}_{T_{\triangle_{odd}}}$, ·–·–■–·–· : $\overline{\psi}_{SG_{\triangle}}$)

Table 4.8: The rotation invariance of the discrete first-order differencing kernels for edge extraction. n_0 denotes that the images are noiseless.

	$T_{\triangle_{even}}$			$T_{\triangle_{odd}}$			$SG_{\triangle}$		
	$\overline{\psi}$	ψ_σ	ψ_{max}	$\overline{\psi}$	ψ_σ	ψ_{max}	$\overline{\psi}$	ψ_σ	ψ_{max}
$I_{1_{n_5}}$	1.00	0.00	1.00	0.55	0.50	1.00	0.55	0.50	1.00
$I_{2_{n_5}}$	1.00	0.00	1.00	0.49	0.50	1.00	0.50	0.50	1.00
$I_{3_{n_5}}$	0.99	0.14	1.41	0.53	0.50	1.00	0.53	0.50	1.00
$I_{4_{n_5}}$	0.97	0.17	1.00	0.50	0.50	1.00	0.51	0.50	1.00
$I_{5_{n_5}}$	0.94	0.28	2.00	0.51	0.50	1.00	0.51	0.50	1.00
$I_{6_{n_5}}$	0.90	0.34	1.41	0.50	0.50	1.00	0.50	0.50	1.00
$I_{7_{n_5}}$	0.81	0.45	1.41	0.49	0.50	1.00	0.49	0.50	1.00
$I_{8_{n_5}}$	0.87	0.44	1.41	0.49	0.50	1.00	0.49	0.50	1.00
$I_{9_{n_5}}$	0.93	0.37	2.00	0.50	0.50	1.00	0.50	0.50	1.00
$I_{10_{n_5}}$	0.99	0.09	1.00	0.50	0.50	1.00	0.50	0.50	1.00

(a) Errors of extracted edge.

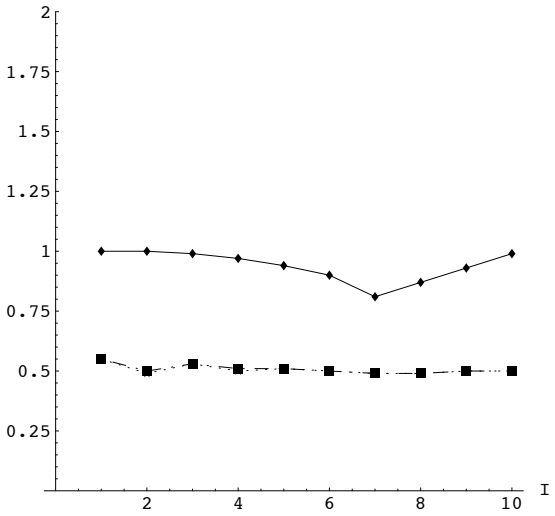

(b) Graphical illustration of $\overline{\psi}$ from $I_{1_{n_5}}$ to $I_{10_{n_5}}$.
(—◆— : $\overline{\psi}_{T_{\triangle_{even}}}$, ⋯★⋯ : $\overline{\psi}_{T_{\triangle_{odd}}}$, ·−·−■−·−· : $\overline{\psi}_{SG_{\triangle}}$)

Table 4.9: The rotation invariance of the discrete first-order differencing kernels for edge extraction. n_5 denotes that the images are weakly noisy (with the additive Gaussian noise of $\sigma = 5.0$)

	$T_{\triangle_{even}}$			$T_{\triangle_{odd}}$			$SG_{\triangle}$		
	$\overline{\psi}$	ψ_σ	ψ_{max}	$\overline{\psi}$	ψ_σ	ψ_{max}	$\overline{\psi}$	ψ_σ	ψ_{max}
$I_{1_{n10}}$	1.00	0.00	1.00	0.53	0.50	1.00	0.52	0.50	1.00
$I_{2_{n10}}$	0.99	0.18	2.00	0.47	0.50	1.00	0.48	0.50	1.00
$I_{3_{n10}}$	0.99	0.26	2.00	0.55	0.50	1.00	0.56	0.50	1.00
$I_{4_{n10}}$	0.93	0.30	2.00	0.51	0.50	1.00	0.50	0.50	1.00
$I_{5_{n10}}$	0.95	0.30	2.00	0.54	0.50	1.00	0.55	0.50	1.00
$I_{6_{n10}}$	0.86	0.40	1.41	0.51	0.50	1.00	0.51	0.50	1.00
$I_{7_{n10}}$	0.82	0.45	1.41	0.46	0.50	1.00	0.46	0.50	1.00
$I_{8_{n10}}$	0.86	0.45	1.41	0.48	0.50	1.00	0.48	0.50	1.00
$I_{9_{n10}}$	0.93	0.39	2.00	0.50	0.50	1.00	0.50	0.50	1.00
$I_{10_{n10}}$	0.94	0.35	1.41	0.50	0.50	1.00	0.50	0.50	1.00

(a) Errors of extracted edge.

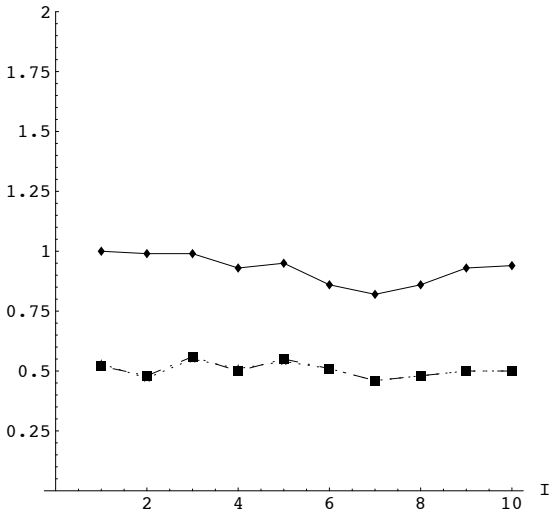

(b) Graphical illustration of $\overline{\psi}$ from $I_{1_{n10}}$ to $I_{10_{n10}}$.
(—◆— : $\overline{\psi}_{T_{\triangle_{even}}}$, ⋯★⋯ : $\overline{\psi}_{T_{\triangle_{odd}}}$, ·−·−■−·−· : $\overline{\psi}_{SG_{\triangle}}$)

Table 4.10: The rotation invariance of the discrete first-order differencing kernels for edge extraction. n_{10} denotes that the images are strongly noisy (with the additive Gaussian noise of $\sigma = 10.0$)

		$T_{\triangle_{even}}$			$T_{\triangle_{odd}}$			$SG_{\triangle}$		
		$\overline{\psi}$	ψ_σ	ψ_{max}	$\overline{\psi}$	ψ_σ	ψ_{max}	$\overline{\psi}$	ψ_σ	ψ_{max}
n_0	$t_E = \frac{3}{3}$	0.34	0.48	1.41	0.25	0.43	1.00	0.25	0.43	1.00
	$t_E = \frac{7}{3}$	0.35	0.49	1.41	0.26	0.44	1.41	0.25	0.44	1.41
	$t_E = \frac{13}{3}$	0.37	0.51	2.24	0.26	0.45	2.24	0.26	0.45	2.24
n_5	$t_E = \frac{3}{3}$	0.37	0.50	1.41	0.25	0.43	1.00	0.25	0.43	1.00
	$t_E = \frac{7}{3}$	0.37	0.51	1.41	0.25	0.44	1.41	0.26	0.44	1.41
	$t_E = \frac{13}{3}$	0.37	0.51	2.24	0.26	0.45	2.24	0.26	0.45	2.24
n_{10}	$t_E = \frac{3}{3}$	0.54	1.82	27.59	0.25	0.43	1.00	0.28	0.58	7.81
	$t_E = \frac{7}{3}$	0.41	0.53	1.41	0.26	0.44	1.41	0.26	0.44	1.41
	$t_E = \frac{13}{3}$	0.42	0.55	2.24	0.26	0.44	1.41	0.26	0.44	1.41

(a) Errors of extracted edge from SE1.

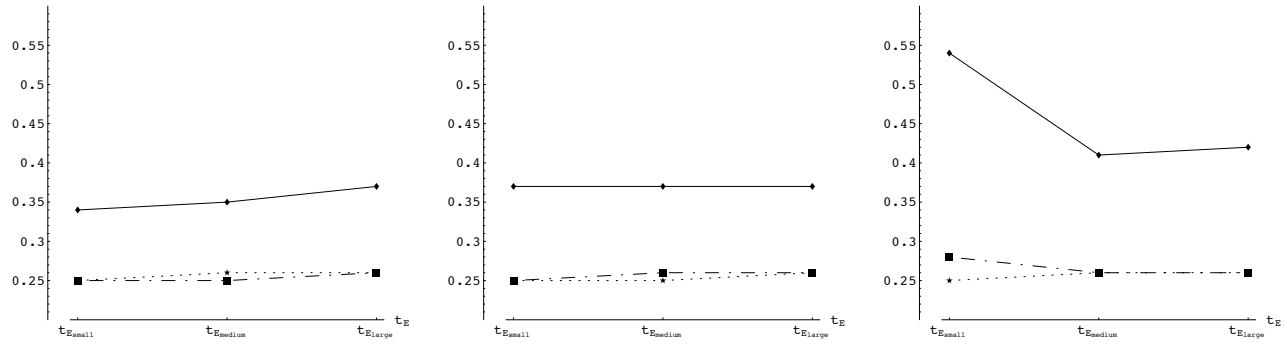

$\overline{\psi}_{n0}$ $\overline{\psi}_{n_5}$ $\overline{\psi}_{n_{10}}$

(b) Graphical illustration of $\overline{\psi}$ (—♦— : $\overline{\psi}_{T_{\triangle_{even}}}$, ⋯★⋯ : $\overline{\psi}_{T_{\triangle_{odd}}}$, · − · − ■ − · − · : $\overline{\psi}_{SG_{\triangle}}$).

Table 4.11: Steadiness from adjacency of the discrete first-order differencing kernels for edge extraction in case of SE1 given in Fig 3.4(a). t_E presents the blurred edge width, and n_0, n_5, and n_{10} denote that the three levels of noise added to SE1, (i.e. n_0 : noiseless, n_5 : the additive Gaussian noise of $\sigma = 5.0$, and n_{10} : the additive Gaussian noise of $\sigma = 10.0$).

		$T_{\triangle_{even}}$			$T_{\triangle_{odd}}$			$SG_{\triangle}$		
		$\overline{\psi}$	ψ_σ	ψ_{max}	$\overline{\psi}$	ψ_σ	ψ_{max}	$\overline{\psi}$	ψ_σ	ψ_{max}
n_0	$t_E = \frac{3}{3}$	0.86	0.38	2.00	0.38	0.49	2.00	0.38	0.49	1.00
	$t_E = \frac{7}{3}$	0.86	0.40	2.00	0.39	0.49	1.00	0.38	0.49	1.00
	$t_E = \frac{13}{3}$	0.86	0.40	2.00	0.40	0.49	1.41	0.40	0.49	1.41
n_5	$t_E = \frac{3}{3}$	0.84	0.41	2.00	0.37	0.49	2.00	0.37	0.49	2.00
	$t_E = \frac{7}{3}$	0.82	0.43	2.00	0.38	0.49	1.00	0.37	0.48	1.00
	$t_E = \frac{13}{3}$	0.82	0.44	2.00	0.40	0.49	1.41	0.41	0.49	1.41
n_{10}	$t_E = \frac{3}{3}$	0.94	1.87	30.00	0.36	0.49	2.00	0.47	1.86	30.00
	$t_E = \frac{7}{3}$	0.80	0.45	2.00	0.38	0.48	1.00	0.36	0.48	1.00
	$t_E = \frac{13}{3}$	0.80	0.47	2.00	0.40	0.50	2.00	0.39	0.50	2.00

(a) Errors of extracted edge from SE4.

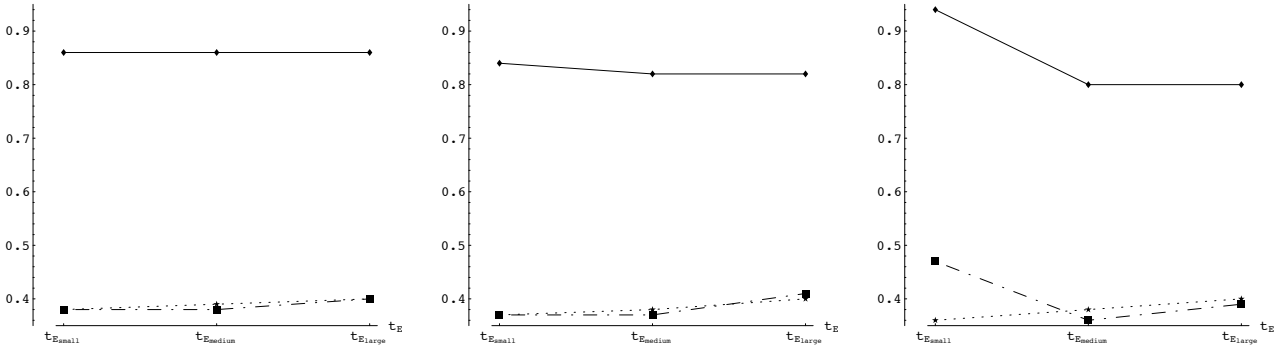

$\overline{\psi}_{n_0}$ $\overline{\psi}_{n_5}$ $\overline{\psi}_{n_{10}}$

(b) Graphical illustration of $\overline{\psi}$ (—◆— : $\overline{\psi}_{T_{\triangle_{even}}}$, ···★··· : $\overline{\psi}_{T_{\triangle_{odd}}}$, - - - ■ - - - : $\overline{\psi}_{SG_{\triangle}}$).

Table 4.12: Steadiness from adjacency of the discrete first-order differencing kernels for edge extraction in case of SE4 given in Fig 3.4(b). t_E presents the blurred edge width, and n_0, n_5, and n_{10} denote that the three levels of noise added to SE4, (i.e. n_0 : noiseless, n_5 : the additive Gaussian noise of $\sigma = 5.0$, and n_{10} : the additive Gaussian noise of $\sigma = 10.0$).

		$T_{\triangle_{even}}$			$T_{\triangle_{odd}}$			$SG_{\triangle}$		
		$\overline{\psi}$	ψ_σ	ψ_{max}	$\overline{\psi}$	ψ_σ	ψ_{max}	$\overline{\psi}$	ψ_σ	ψ_{max}
n_0	$t_E = \frac{3}{3}$	0.78	0.42	1.41	0.37	0.48	1.00	0.37	0.48	1.00
	$t_E = \frac{7}{3}$	0.79	0.47	2.00	0.45	0.50	1.00	0.43	0.49	1.00
	$t_E = \frac{13}{3}$	0.84	0.50	2.00	0.50	0.50	1.41	0.50	0.50	1.41
n_5	$t_E = \frac{3}{3}$	0.76	0.43	1.41	0.40	0.49	1.00	0.40	0.49	1.00
	$t_E = \frac{7}{3}$	0.79	0.47	2.00	0.43	0.49	1.00	0.44	0.50	1.00
	$t_E = \frac{13}{3}$	0.84	0.49	2.00	0.50	0.51	1.41	0.49	0.50	1.41
n_{10}	$t_E = \frac{3}{3}$	0.95	2.21	30.00	0.40	0.49	1.41	0.53	1.96	30.00
	$t_E = \frac{7}{3}$	0.78	0.48	2.00	0.43	0.50	1.00	0.44	0.50	1.00
	$t_E = \frac{13}{3}$	0.86	0.47	2.00	0.50	0.51	1.41	0.50	0.51	1.41

(a) Errors of extracted edge from CE1.

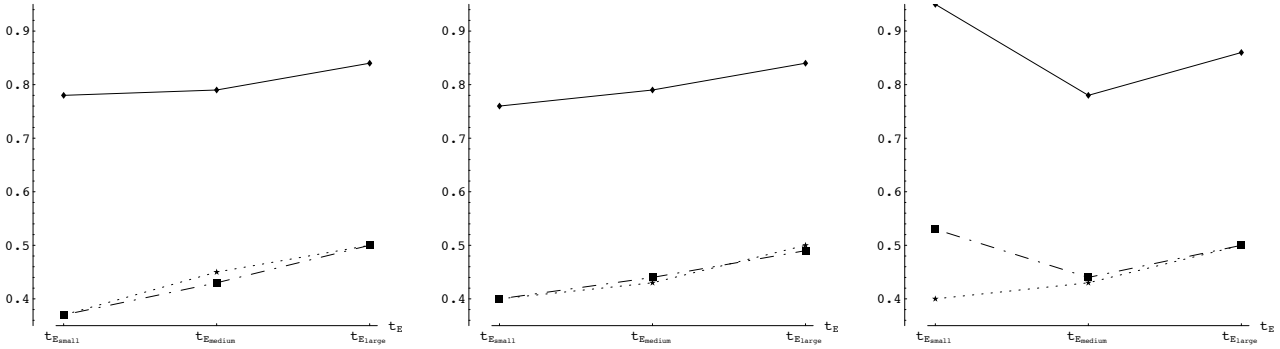

$\overline{\psi}_{n_0}$ $\overline{\psi}_{n_5}$ $\overline{\psi}_{n_{10}}$

(b) Graphical illustration of $\overline{\psi}$ (—◆— : $\overline{\psi}_{T_{\triangle_{even}}}$, ···★··· : $\overline{\psi}_{T_{\triangle_{odd}}}$, - - - -■- - - - : $\overline{\psi}_{SG_{\triangle}}$).

Table 4.13: Steadiness from adjacency of the discrete first-order differencing kernels for edge extraction in case of CE1 given in Fig 3.4(c). t_E presents the blurred edge width, and n_0, n_5, and n_{10} denote that the three levels of noise added to CE1, (i.e. n_0 : noiseless, n_5 : the additive Gaussian noise of $\sigma = 5.0$, and n_{10} : the additive Gaussian noise of $\sigma = 10.0$).

		$T_{\triangle_{even}}$			$T_{\triangle_{odd}}$			$SG_{\triangle}$		
		$\overline{\psi}$	ψ_σ	ψ_{max}	$\overline{\psi}$	ψ_σ	ψ_{max}	$\overline{\psi}$	ψ_σ	ψ_{max}
n_0	$t_E = \frac{3}{3}$	0.60	0.51	1.41	0.30	0.46	1.00	0.30	0.46	1.00
	$t_E = \frac{7}{3}$	0.60	0.53	2.00	0.34	0.47	1.00	0.34	0.47	1.00
	$t_E = \frac{13}{3}$	0.63	0.56	2.00	0.36	0.48	1.41	0.36	0.48	1.41
n_5	$t_E = \frac{3}{3}$	0.59	0.52	2.00	0.33	0.47	1.00	0.34	0.47	1.00
	$t_E = \frac{7}{3}$	0.59	0.53	2.00	0.34	0.47	1.00	0.34	0.47	1.00
	$t_E = \frac{13}{3}$	0.62	0.54	2.00	0.37	0.48	1.41	0.37	0.48	1.41
n_{10}	$t_E = \frac{3}{3}$	0.76	1.99	30.00	0.34	0.47	1.00	0.38	0.81	12.08
	$t_E = \frac{7}{3}$	0.59	0.53	2.00	0.35	0.48	1.00	0.37	0.48	1.00
	$t_E = \frac{13}{3}$	0.61	0.54	2.00	0.38	0.49	1.41	0.37	0.48	1.00

(a) Errors of extracted edge from CE4.

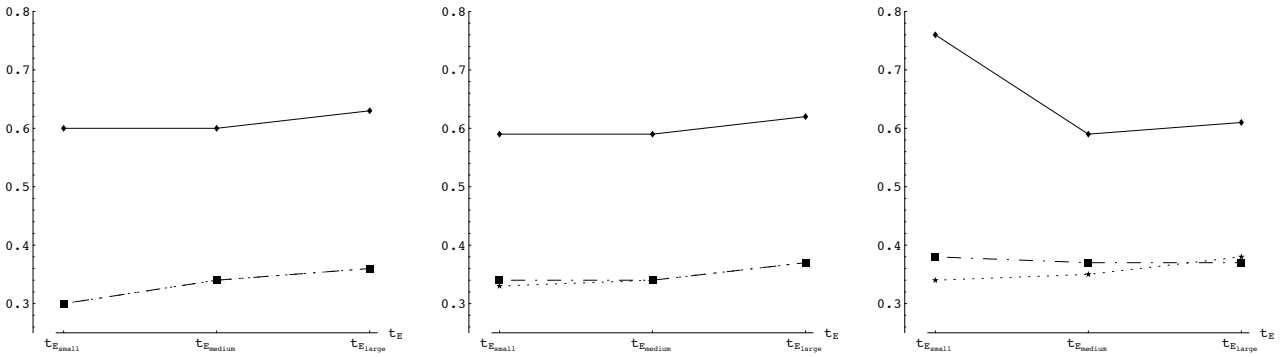

$\overline{\psi}_{n_0}$ $\overline{\psi}_{n_5}$ $\overline{\psi}_{n_{10}}$

(b) Graphical illustration of $\overline{\psi}$ (—◆— : $\overline{\psi}_{T_{\triangle_{even}}}$, ···★··· : $\overline{\psi}_{T_{\triangle_{odd}}}$, - - - ■ - - - : $\overline{\psi}_{SG_{\triangle}}$).

Table 4.14: Steadiness from adjacency of the discrete first-order differencing kernels for edge extraction in case of CE4 given in Fig 3.4(d). t_E presents the blurred edge width, and n_0, n_5, and n_{10} denote that the three levels of noise added to CE4, (i.e. n_0 : noiseless, n_5 : the additive Gaussian noise of $\sigma = 5.0$, and n_{10} : the additive Gaussian noise of $\sigma = 10.0$).

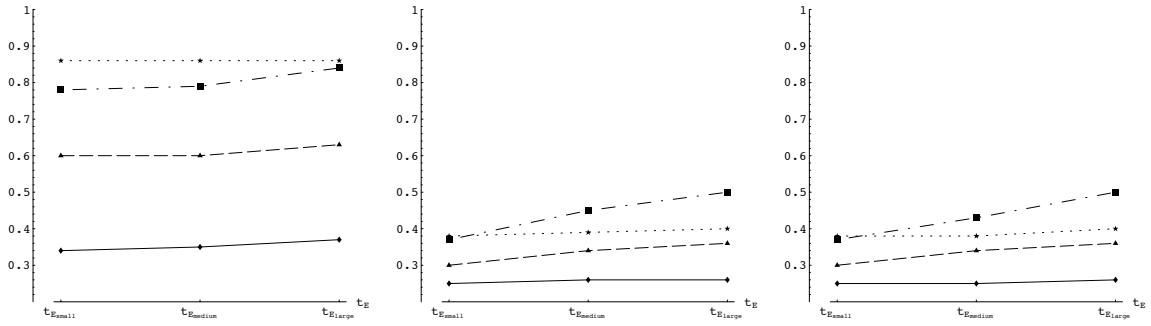

(a) $\overline{\psi}_{n_0,T_{\triangle_{even}}}$ (b) $\overline{\psi}_{n_0,T_{\triangle_{odd}}}$ (c) $\overline{\psi}_{n_0,SG_{\triangle}}$

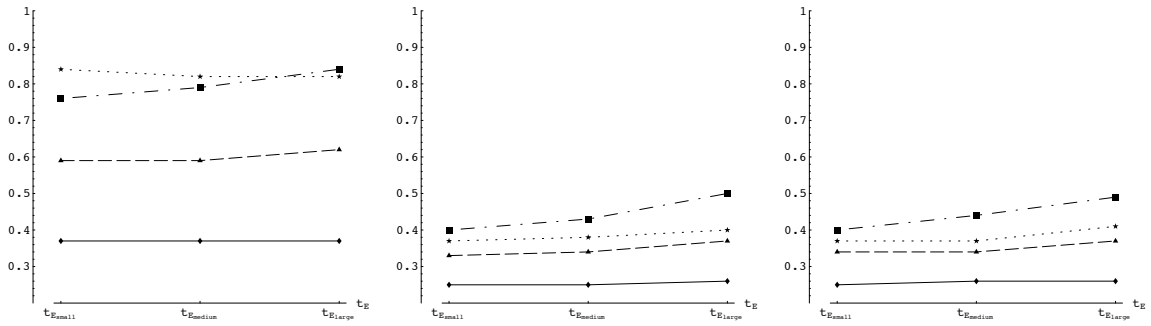

(d) $\overline{\psi}_{n_5,T_{\triangle_{even}}}$ (e) $\overline{\psi}_{n_5,T_{\triangle_{odd}}}$ (f) $\overline{\psi}_{n_5,SG_{\triangle}}$

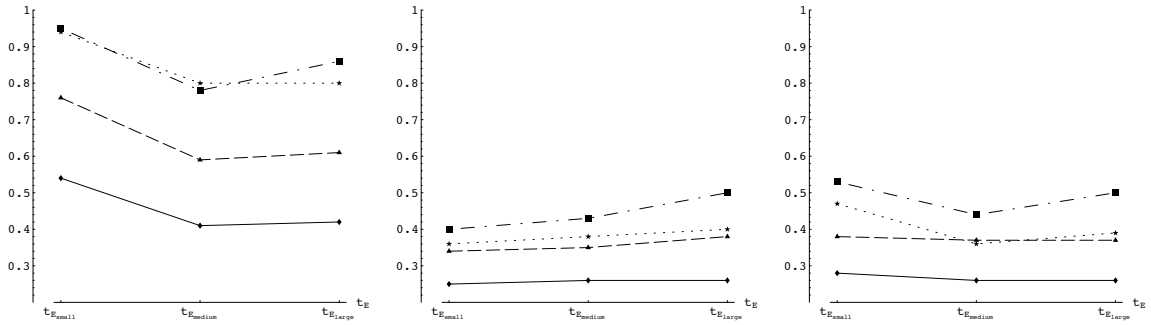

(g) $\overline{\psi}_{n_{10},T_{\triangle_{even}}}$ (h) $\overline{\psi}_{n_{10},T_{\triangle_{odd}}}$ (i) $\overline{\psi}_{n_{10},SG_{\triangle}}$

Figure 4.5: Error of edge extraction applied to the images in Fig 3.5. Each row differs in the level of noise and each column differs in the type of the used discrete first-order differencing kernel (—♦— : SE1, ···★··· : SE4, · – · – ■ – · – · : CE1, – – –▲– – – : CE4).

4.4 Summary

We give here a brief summary of the main results of the validation study as follows:

- Accuracy of approximation : $T(x;t)$ is superior to $SG(x;t)$.
- Fulfillment of the non-enhancement requirement : $T(x;t)$ and $SG(x;t)$ both fulfill the non-enhancement requirement.
- Accuracy of edge extraction
  - Rotation invariance : $T_{\triangle_{even}}$ is inferior to $T_{\triangle_{odd}}$ and to $SG_{\triangle}$.
  - Steadiness from adjacency :
    - $T_{\triangle_{even}}$is generally inferior to $T_{\triangle_{odd}}$ and to $SG_{\triangle}$.
    - In the case of $t_{E_{small}}$ with n_{10}, $T_{\triangle_{odd}}$ is obviously superior to $SG_{\triangle}$.
    - SE1 (CE4) is the steadiest (the second steadiest) image type.

As a consequence, our derived DSS kernel does not only match the performance of the commonly used SG kernel but also clearly exhibits superior performance with respect to smoothing and differentiation.

5 Conclusion

In this report, we closely investigated the properties of the derived DSS kernel compared with the SG kernel, and presented the results of a validation study in which the performance of the DSS kernel compared with that of the SG kernel is characterized with respect to accuracy of approximation, to fulfillment of the non-enhancement requirement, and to accuracy of edge extraction divided into two subcriteria, namely rotation invariance and steadiness from adjacency.

With regard to the sampled Gaussian kernel, several problems have been observed. First, it was shown in [13] that a sampled Gaussian can lead to undesirable effects. Moreover, one can see from the mathematical derivation in [10, Sec. 4] that a sampled Gaussian of a small scale is not appropriate for approximating the continuous Gaussian. Furthermore, according to our investigation in Section 2, the sampled Gaussian is not always normalized both for smoothing and for differentiation, whereas the DSS kernel is always normalized for any scale.

The result of our validation study proves that i) $SG(x;t)$ is not superior to $T(x;t)$ with respect to approximation for discrete convolution when t gets smaller, ii) the DSS kernel as well as the SG kernel fulfills the non-enhancement requirement, and iii) regarding accuracy of edge extraction, $T_{\triangle_{even}}$ is generally inferior to $T_{\triangle_{odd}}$ and to $SG_{\triangle}$ with respect to rotation invariance as well as to steadiness from adjacency.

Consequently, we conclude that our derived DSS kernel does not only match the performance of the commonly used SG kernel but also clearly exhibits superior performance with respect to smoothing and differentiation.

References

[1] R. N. Bracewell. *The Fourier Transform and Its Applicationss;thrid edition.* McGraw-Hill, 2000.

[2] I. N. Bronstein and K. A. Semendjajew. *Teubner-Taschenbuch der Mathematik.* B. G. Teubner, Stuttgart, 1996.

[3] J. F. Canny. A computational approach to edge detection. *IEEE Trans. on Pattern Analysis and Machine Intelligence*, 8(6):679–698, 1986.

[4] E. R. Dougherty. *Probability and Statistics for the Engineering, Computing, and Physical Sciences.* Prentice-Hall, Inc., Englewood Cliffs, New Jersey, 1990.

[5] N. Fliege. *Systemtheorie.* Informationstechnik. Teubner, Stuttgart, 1991.

[6] L. M. J. Florack. *Image Structure.* Kluwer Academic Publishers, Dordrecht, The Netherlands, 1997.

[7] J. W. Harris and H. Stocker. *Handbook of Mathematics and Computational Science.* Springer, 1998.

[8] R. A. Johnson and D. W. Wichern. *Applied Multivariate Statistical Analysis.* Prentice Hall, Inc., Upper Saddle River, New Jersey, 1998.

[9] J. Y. Lim. On the Role of the Gaussian Kernel in Edge Detection and Scale-Space Methods. Technical Report FBI-HH-B-230/01, Fachbereich Informatik, Universität Hamburg, Germany, 2001.

[10] J. Y. Lim. On the Discrete Scale-Space Formulation. Technical Report FBI-HH-B-231/01, Fachbereich Informatik, Universität Hamburg, Germany, 2001.

[11] J. Y. Lim. The Supplemented Discrete Scale-Space Formulation. Technical Report FBI-HH-M-312/02, Fachbereich Informatik, Universität Hamburg, Germany, 2002.

[12] J. Y. Lim. On Higher Dimensional Multiscale Edge Extraction. Technical Report FBI-HH-B-238/02, Fachbereich Informatik, Universität Hamburg, Germany, 2002.

[13] T. Lindeberg. Scale-Space for Discrete Signals. *IEEE Trans. on Pattern Analysis and Machine Intelligence*, 12(3):234–264, 1990.

[14] P. A. Lynn and W. Fuerst. *Digital Signal Processing with Computer Application;second edition.* John Wiley & Sons, 1997.

[15] A. V. Oppenheim and R. W. Schafer with J. R. Buck. *Discrete-Time Signal Processing, 2nd Edition.* Prentice Hall International, Inc., Upper Saddle River, New Jersey, 1999.

[16] K. Rohr. Recognizing corners by fitting parametric models. *Internat. Journal of Computer Vision*, 9(3):213–230, 1992.

[17] S. Wolfram. *Mathematica, 2nd Edition.* Addison-Wesley Publishing Company, 1991.